Magnesium Twin Roll Casting Machine - *Modelling and Control*

Osama A. Alguefer

Department of Electrical & Computer Engineering
McGill University
Montreal, Canada

October 2012

A thesis submitted to McGill University in partial fulfillment of the requirements for the degree of Masters in Electrical Engineering.

2012/10/05

Abstract

In this thesis, a laboratory scale-pilot twin roll casting plant at CANMET-MTL is considered for modelling for control synthesis. Three important parts of the plant are considered for modelling: feeding system, solidification process and deformation process. The TRC machine is multi-input multi-output (MIMO) and nonlinear in nature. A simplified 2×2 feedback linear dynamical model is developed based on first principles and engineering intuition due to the lack of experimental data from the TRC machine. The proposed manipulated variables are the melt inflow rate and rollers angular velocity whereas the corresponding controlled variables are the head-box melt level and roll separating force. In this model, the effect of metallostatic pressure on solidification front position is modelled as a spring-damper mechanical system. Different parameter values of the first-order model are empirically tested until smooth movement of the solidification fronts is obtained. Casting speed is optimized using a theoretical model validated using numerical simulation data. The proposed model is mainly used to control the roll separating force in steady-state and maintain nominal performance. Therefore, simple proportional-integral (PI) decentralized controllers are designed using a trial-and-error method as a first attempt to control the process. Then a design of multivariable $\mathcal{H}_\infty$ optimal control is carried out using MATLAB *hinfsyn* function.

Résumé

Dans cette thèse, un procédé pilote de coulée en bande à double rouleau de magnésium du laboratoire CANMET-MTL est considéré pour la modélisation orientée pour la conception de contrôleurs. Trois sections importantes de ce procédé sont considérées pour la modélisation: le système d'alimentation, le processus de solidification et le processus de déformation. La machine de coulée à double rouleau (twin-roll casting-TRC) est de nature multientrées-multisorties et non linéaire. Un modèle dynamique linéaire simplifié 2×2 est développé en se basant sur des principes physiques et une intuition d'ingénierie dû au manque de données expérimentales sur la machine TRC. On propose les variables manipulées comme étant le débit d'entrée de métal en fusion ainsi que la vitesse angulaire des rouleaux, alors que les variables contrôlées correspondantes sont le niveau de liquidus dans la boîte d'alimentation et la force de séparation des rouleaux. Dans ce modèle, l'effet de la pression métallostatique sur la position du front de solidification est modélisé par un système mécanique composé d'un ressort et d'un amortisseur. Différentes valeurs de paramètres de ce modèle de premier ordre sont testées de façon empirique jusquà ce qu'un mouvement sans à-coups du front de solidification soit obtenu. La vitesse de coulée est optimisée en utilisant un modèle théorique validé par l'utilisation de données de simulation numérique. Le modèle développé est utilisé principalement pour réguler la force de séparation des rouleaux en régime permanent et pour maintenir la performance nominale. En conséquence, de simples régulateurs décentralisés de type proportionnel-intégral (PI) sont conçus en guise de premier essai pour contrôler le procédé. Puis, un contrôleur multivariable H-infini est conçu en utilisant la fonction *hinfsyn* dans Matlab.

Acknowledgements

First, I would sincerely thank my supervisor Prof. **Benoit Boulet** for his support and positive feedback; without him this thesis would not have come into being. I would also thank him for the opportunity he gave me to work on this project.

I would extent a word of thanks to Dr. **Elhachmi Essadiqi** of CANMET-MTL Hamilton, Ontario. He helped me understanding the machine's operation and provided me with the dimensions of the machine's parts. His advice, help and experience are greatly appreciated.

I am much grateful to Ph.D. student Mr. **Amir Haddadzadeh** at the University of Waterloo, who is working on developing a numerical model for the CANMET-MTL Twin Roll Caster for simulation purposes. He provided me with some simulation data that was used in this thesis. His help is highly acknowledged and appreciated.

I am so grateful to the Libyan educational and scientific program for the scholarship and to the CBIE (Canadian Bureau for International Education) who amazingly administered the Libyan scholarship program during the Libyan uprising.

I must also acknowledge McGill University services. Of particular, Schulich library and McGill centre for intelligent machines.

Finally, I am indebted to my family for their love and support ♡.

McGill Centre for Intelligent Machines,
3480 University, Montreal,
Quebec, Canada H3A 0E9

Osama Alguefer
October 2012

To my family and free Libya ♡

> "One's mind, once stretched by a new idea, never regains its original dimensions."
>
> — *Oliver Wendell Holmes*

Contents

List of Figures

List of Tables

List of Acronyms

CANMET-MTL	CANMET Materials Technology Laboratory
CFD	Computational Fluid Dynamics
CSIRO	Commonwealth Scientific & Industrial Research Organization
HB	Head-Box
HTRC	Horizontal Twin Roll Caster
MIMO	Multi-input Multi-output
PI	Proportional Integral controller
PLC	Programmable Logic Controller
POSCO	Pohang Iron & Steel Company
RGA	Relative Gain Array
RSF	Roll Separating Force
TFM	Transfer Function Matrix
TRC	Twin Roll Casting
VTRC	Vertical Twin Roll Caster

Chapter 1

Introduction

1.1 Historical Background

The general idea of twin roll strip casting goes back to 1856 when the first twin roll strip caster to produce thin strip products was invented and patented by Sir Henry Bessemer [4]. Fig. 1.1 depicts the schematic representation of Bessemer's caster. The twin roll strip casters did not become industrial practice until the 1950's, owing to a number of practical problems such as: thermal stresses of the rolls, homogeneous delivery of the molten metal to the cooled rotating rolls to preclude the uneven solidification of the molten metal and premature solidification in the nozzle tip and cooling methods. In addition to the practical problems, "technical components such as measurement devices and [industrial] computer control technology [like programmable logic controllers (PLC)] were not available at that time" [5]. However, Bessemer's concept paved the way for today's commercial casters.
The rapid consumption of aluminum to meet the demand of the post-war economic boom of car and military aircraft productions triggered the need to produce thin strips and foil alloys at low cost and helped develop twin roll casting processes on the basis of Bessemer's

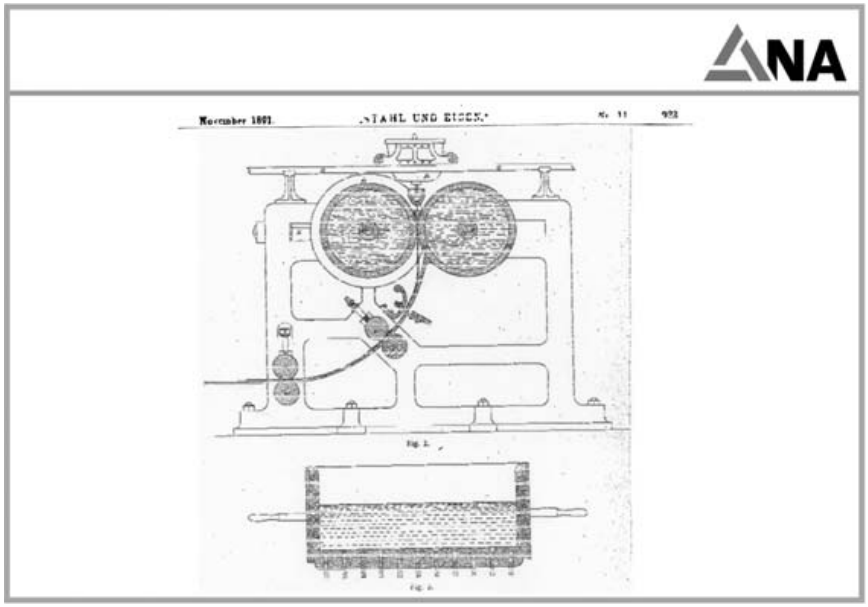

Fig. 1.1 Schematic diagram of Bessemer's twin roll strip caster, adapted from[1]

principle. Thus, after many years of R& D efforts expended on laboratory scale pilot twin roll casters, the first successful commercial twin roll caster was developed by Pechiney Aluminum Engineering in France and by Hunter Engineering Co. (currently FATA Hunter Inc.) in the U.S.A in 1956 [6][7]. However, the Pechiney aluminum twin roll caster had to run at low speeds to preserve strip quality requirements. Moreover, the produced strips were of large gauge thickness. In parallel to Pechiney's development program, the American Hunter Engineering Co. managed in the 1970-90's to develop a caster called $Supercaster^{TM}$ capable of casting thin gauge strips at high casting speeds. Also, in the 1970-90's Pechiney developed aluminum casters called $JAMPO\ 3C^{TM}$ and $JAMPO\ 3CM^{TM}$. The French Pechiney's casters, however, can be easily distinguished from Hunter's in terms of design, performance and productivity [8][9].

In the steel-making industry, it is difficult to ascertain when the first commercial steel

twin roll caster was successfully commissioned due to commercial reasons. However, the development of steel twin roll caster since the 1980's had encountered several challenges such as the high melting point and density of steel and a relative low thermal conductivity compared with aluminum.

For magnesium twin roll casting, Commonwealth Scientific & Industrial Research Organization (CSIRO), in Australia, has been developing scale-pilot twin roll caster of magnesium alloy since 2000 and after few years of research and development work conducted on a scale-pilot caster, CSIRO has successfully produced magnesium strips of 600 mm width and 2.5 mm thickness [10]. Therefore, CSIRO is expected to take the process, if it has not already been done, to the commercial stage in near future. In Canada, strip casting of magnesium alloy is currently at the pilot scale practice.

1.2 Twin Roll Casting Process

The possibility of producing solid strips of different thicknesses and widths directly from molten metal has generated wide interest in academia and metal-making industries due to many advantages such as low capital cost, energy savings and high productivity. The molten metal can be either horizontally or vertically fed into a pair of cooled, rapidly rotating rolls. Twin roll casting processes have created a revolution in metal industries by producing metal strips and foil products at considerably low cost compared with conventional continuous casting processes such as slab/mold continuous casting. Fig 1.2 depicts schematic diagram of continuous slab casting process and continuous twin roll casting process [2]. It can be seen from Fig. 1.2(b) that there is a major reduction in the subsequent hot rolling needed during the conventional casting production. Therefore, savings on both cost and energy consumption is achieved. Moreover, the energy savings makes the twin roll

casting process an environmentally friendly process. Twin roll casters are characterized by rapid solidification rate because the solidification time is very short compared with conventional slab casters and the solidification process takes place on two roll surfaces. This characteristic enables significantly higher production rate (i.e. high casting speeds) [11]. Thus, twin roll casting (TRC) processes have the advantages of cost, energy savings and high productivity.

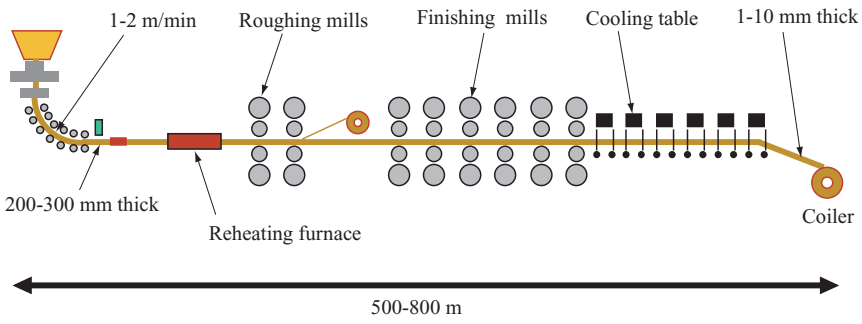

(a) Continuous slab/mold casting process

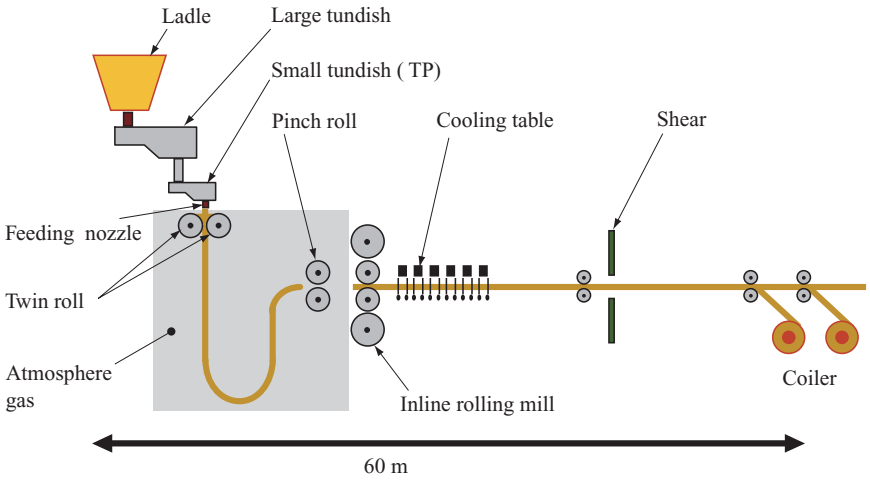

(b) Continuous strip twin roll casting process

Fig. 1.2 Schematic diagram of continuous slab caster and strip twin roll caster, adapted from[2]

The way the molten metal is delivered to the rotating rolls distinguishes two principle twin roll strip casting techniques that are vertical-type twin roll strip casting (VTRC) and horizontal-type twin roll strip casting (HTRC). Fig. 1.3 illustrates the schematic representation of the basic casting configurations. Of the two techniques, the former is the most common technique in the literature and in the ferrous metal industry because of its high rate of productivity [1], whereas the latter is commonly used in aluminum industry. However, both has its own advantages and disadvantages, but the concept of operations for both settings remains the same.

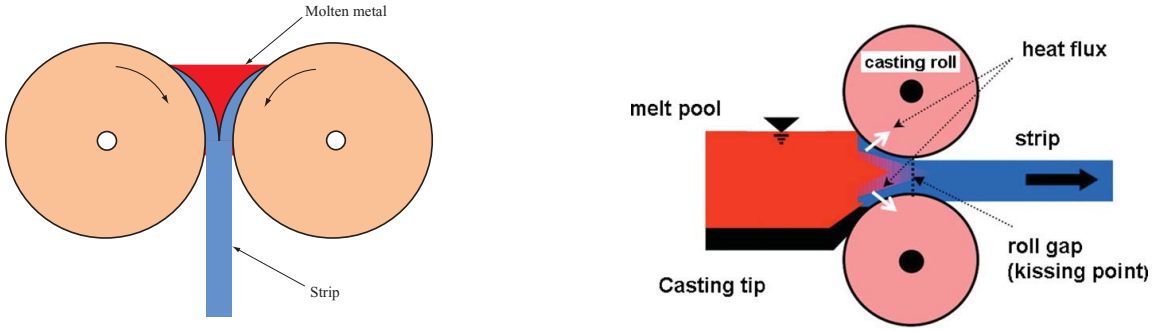

(a) Vertical-type twin roll caster, adapted from[2]

(b) Horizontal-type twin roll caster, adapted from[12]

Fig. 1.3 Basic configurations of twin roll casters

1.2.1 Twin Roll Strip Casting Process of Magnesium Alloys

The twin roll casting process combines solidification and deformation in a single step. Although twin roll casting is an old concept, applying twin roll casting technology to magnesium alloys is relatively new and difficult compared with other metals and alloys such as steel and aluminum. It is expected for magnesium and its alloys to be the 21^{st} century material owing to their intriguing mechanical properties. However, some of their thermal properties impose challenges on strip casting process. Like aluminum, the typical

arrangement of magnesium twin roll casting is the horizontal-type setting.

Magnesium is expected to take over steel and aluminium in many metal industries due to its favourable mechanical properties. Magnesium and magnesium alloys have intriguing properties of tensile strength, elastic modulus, low density (i.e. high strength to weight ratios) and high damping characteristics. Moreover, magnesium makes good shield against unwanted electromagnetic waves and provides effective dissipation of heat. These properties are of profound interest in communication, electronic and computer industries [10] [11]. Nevertheless, It could be a bit of a challenge using magnesium and its alloys in industry through strip casting because of their thermal properties. For example, magnesium and its alloys are easily oxidized and show large segregation effects upon solidification because of their high solidification rate compared with aluminium alloys. Also, molten magnesium freezes faster than molten aluminum. Therefore, very technical twin roll casting methods have to be developed in order to reduce the exposure to the air as much as possible and control the interfacial heat transfer to obtain uniform solidification rate [13] [8]. Having these challenges being met and the manufacturing cost taken into account, magnesium and its alloys are one of the emerging and promising materials. Unlike steel and other metals which use vertical twin roll casters, Magnesium strips are typically produced using horizontal twin roll casters, which are more challenging. It is difficult to preclude molten magnesium from oxidation in the vertical-type setting as a result of the exposure to the air using mix-gas supply. For this reason and more, the magnesium is rolled horizontally.

Chapter 2

Literature Survey

Twin roll casting machines (TRC) have found wide acceptance in ferrous and non-ferrous metal industries for producing cast strips of different thicknesses and widths, owing to its high productivity, low cost and energy savings. The twin roll casting process is a combined solidification/deformation technique compared with conventional casting processes such as continuous mold/slab casting processes, which are solidification only with no hot deformation [14]. In vertical steel twin roll caster, the space formed by the rollers works as a melt mass storage and the melt is distributed along the width of the rolls. Therefore, the level control is done in the melt pool over the rolls. On the contrary, in the magnesium horizontal laboratory scale-pilot twin roll casting machine that is housed at the CANMET Materials Technology Laboratory (CANMET-MTL) in Hamilton, Ontario, the level control is performed in the head-box which is distant from the entrance of the rolls by a refractory nozzle and the width of the produced strip is determined by the face width of the nozzle. For vertical steel twin roll casting processes, stabilizing the melt pool level is of great importance [15][13]. Therefore, it has been targeted by several researchers and a number of advanced control techniques have been investigated. Lee et al. [16][17] adopted

an adaptive fuzzy control technique to regulate the molten steel level of a strip casting system. The feasibly of the proposed controller was demonstrated by carrying out several simulations. In different study by LEE et al., a linearized model with parametric uncertainty of nonlinear time delay molten steel level system of POSCO steel strip caster has been formulated and used for robust control design [15]. Park and Cho [5] proposed a fuzzy logic controller to control the melt level with an emphasis on the interaction between melt level and roll gap variations. Apart from melt level control, there are other control tasks in twin roll casting processes such as strip thickness control, roll gap control, force control, cooling control and exit strip tension control. Bernhard et al. and Simon et al. [18][19] developed a nonlinear state-space model for a laboratory vertical-type steel twin roll caster and proposed a single-loop force controller; gain schedule proportional plus integral (PI) controller to maintain constant strip thickness. Recent works by Hong et al. [20][21] have proposed two-level control strategy to obtain uniform strip thickness and maintain constant roll separating force. Three local controllers are proposed for the melt pool level, roll speed and roll gap. A supervisory controller is designed to deal with interactions between each control loop and provide suitable set-point for the local roll speed controller. In order to study interaction and/or coupling among control variables of vertical twin roll strip casting process, Alberto and John [22][23][24] derived a simplified linear multivariable dynamic model. Although there have been many patents obtained and relatively large amount of research done on twin roll casting technology of steel and aluminum alloys, information and results on twin roll casting processes are very rare in open literature due to commercial sensitivity and competition [8][21]. On the basis of the foregoing literature review, previous research in this field has been limited to steel vertical-type twin roll caster with much attention being paid to melt pool level control. It would be of interest to look at new metal making processes such as horizontal-type twin roll casting process of magnesium alloys.

2.1 Thesis Contribution and Aim

To the best of our knowledge, this is the first time a horizontal-type twin roll casting machine is considered for modeling and control. The main contribution of this thesis is formulating a simple linear multivariable model for the CANMET-MTL machine. In addition, an effort is made to find the "optimal" range of the casting speed, which is of paramount importance in defining exit strip quality and thickness, using a mathematical model equation that is verified using numerical simulation results.

The primary aim of this thesis is understanding the fundamental dynamics involved in the process of interest and then developing a linear multivariable dynamic model that captures the fundamental dynamics of a horizontal twin roll caster (HTRC). For this objective, the pilot-scale twin roll caster at the CANMET-MTL in Hamilton, Ontario is considered for modeling and control synthesis. A secondary aim is adopting the linear multivariable dynamic model to design a controller that provides stable and an acceptable performance for set-point tracking using different methodologies such as classic control and $\mathcal{H}_\infty$ control.

2.2 Thesis Roadmap

The remainder of the thesis is organised as follows. Chapter 3 introduces a brief description of CANMET-MTL strip casting machine and presents detailed mathematical description of the CANMET-MTL strip casting machine. Analysis and control design are carried out in Chapter 4. Chapter 5 summarizes salient results and concludes the thesis.

Chapter 3

Plant Description and Mathematical Modelling

3.1 Plant Description

CANMET-MTL Scale-Pilot Twin Roll Casting of Magnesium Alloys

The CANMET-Materials Technology Laboratory (CANMET-MTL), in Hamilton, Ontario is Canada's largest research center, which focuses on a variety of industrial areas such as transportation, energy and metal manufacturing [25]. The center has an ongoing research conducted on magnesium sheet and its alloys. A laboratory scale-pilot twin roll casting machine housed at the CANMET-MTL is used to produce coilable magnesium strip directly from the molten metal. Magnesium alloy such as AZ31 (i.e. 3% aluminium and 1% zinc) is melted in a melting furnace. The molten magnesium is pumped into a head-box which is distant from a pair of rotating cooling rolls by a refractory nozzle. Thus, at a pouring casting temperature of 700^{o}C, the molten metal is discharged out of the head-box throughout the nozzle tip into the void between the cooled rotating rolls. Solidification process commences

at the point of first metal roll contact and proceeds inward at a rate that varies along the contact length. However, the solidification process should end before the point of minimum clearance between the rolls (kiss point of the rolls) so that a completely solid strip is produced. The solidification takes place on both surfaces of the rolls by forming two solidified shells. The two solidified shells are bonded and hot rolled to produce a coilable solid strip. Considering the foregoing technical problems involved in magnesium casting process in order to preclude any premature solidification in any metal-contacting parts, transfer pipes between the pump and the head-box and from the head-box to the nozzle tip and the head-box itself are electrically preheated. Furthermore, for protection of the molten metal in the head-box against oxidation, the head-box is supplied with mix-gas. Fig. 3.1 shows the CANMET-MTL TRC machine in operation. Further description on the plant (process) and its operation is given in the next sections.

Fig. 3.1 TRC machine in operation at CANMET-MTL Hamilton, Ontario [3]

3.2 Mathematical Modelling

3.2.1 Introduction

Mathematical modelling is a prerequisite for control system design. A mathematical model can be either formulated for simulation purposes (understanding the physical phenomena involved in the process of interest, improving certain design and optimizing process variables) or for control design purposes by capturing the fundamental dynamics. The former models are usually of high order dimension (i.e. $> 10^4$), which are not adequate for control synthesis. In literature on twin roll casting, much attention has been paid to mathematical models for simulation purposes. Broadly speaking, mathematical models of

continuous casting process (also referred to as numerical models) are used to help design optimum continuous casting processes by developing efficient numerical tools to elucidate the coupled flow and heat transfer mechanism and/or to help define the optimal operating conditions by investigating the effects of processing parameter changes without the safety and cost concerns that could result from conducting real experiments [26][27][12][28]. In this chapter, a linear multivarible dynamic model that captures the fundamental dynamics of CANMET-MTL twin roll casting process for control synthesis will be formulated. There are two approaches for developing a mathematical model for control synthesis: first principles modelling technique which can be used if we know the physics and math behind the dynamical behaviour of the process in question and data-driven modelling technique (system identification) which can be used when large scale test data is available and easy to collect (i.e. measurements of processing variables are feasible). Since large scale test data is not yet available or might be difficult at this stage to collect for CANMET-MTL twin roll casting process, the former technique will be used.

3.2.2 Plant Model

3.2.2.1 General Description of the Plant Model

The Twin Roll Casting (TRC) machine combines both solidification and deformation process to achieve the metallurgical structure of the deformed strip in a single step. From a process (plant) analysis point of view, three major parts of the process are considered for modelling: delivering system (Head-Box and its furniture), solidification process and deformation process. The roll gap dynamics and exit strip tension, however, are not on the radar scale of this thesis. Therefore, following CANMET-MTL lab, the roll gap is assumed to be stiff. The underling system (plant) is multi-input multi-output (MIMO) and

nonlinear in nature. Therefore, each part of the three major parts (subsystem) is modeled and linearized around its operating point and then the entire linear model is presented as a combination of the linearized subsystems. A general block diagram depicted in Fig. 3.2 shows the entire plant model and how the three major parts (i.e. linearized subsystems) are interconnected. The proposed manipulated variables of the plant are volumetric inflow rate of the molten metal Q_{in} and the angular velocity of the rolls Ω_r whereas the corresponding output variables are the melt level in the head-box h and the roll separating force F, which is exerted on the rolls due to the joining of the two solidified shells. For quality aspects, the position of solidification fronts x_s is also of interest. The broader picture and idea of the plant model is borrowed from [23].

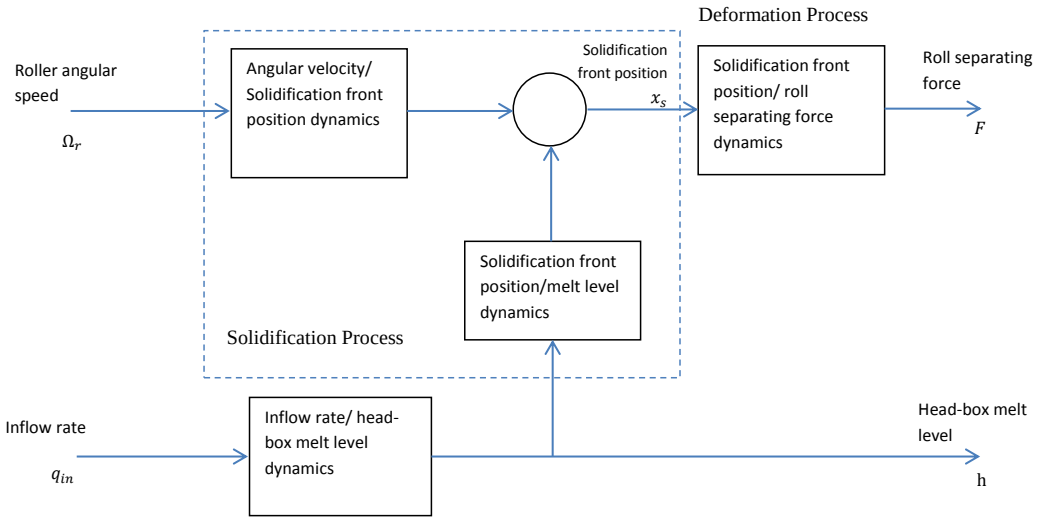

Fig. 3.2 A schematic block diagram of the plant model

3.2.2.2 Head-Box Melt Level Model

The Magnesium melt level in the head-box (HB) is of great importance for the final strip thickness and quality. The exit nozzle pressure, which determines the meniscus position, is regulated by control of the melt level in the head-box. In continuous casting a constant melt flow is desired, which can be fulfilled by control of the melt level in the head-box [13]. There are three different levels in the head-box that are high level, casting (working) level and low level. The process (plant) is mainly working under the supervision of an industrial control system such as PLC (Programmable Logic Controller). At start-up operation a baffle valve in the head-box is pneumatically and fully opened, when the high level is obtained, using a PLC command so as to fill a preheated transfer pipe and tip nozzle. Consequently, head-box melt level drops to the working level which is kept constant during the entire casting run. Upon opening the baffle valve, the casting process is launched. The baffle valve remains fully open during a casting run and has no role in controlling the melt level in the head-box. The level in question therefore is the working level which is considered

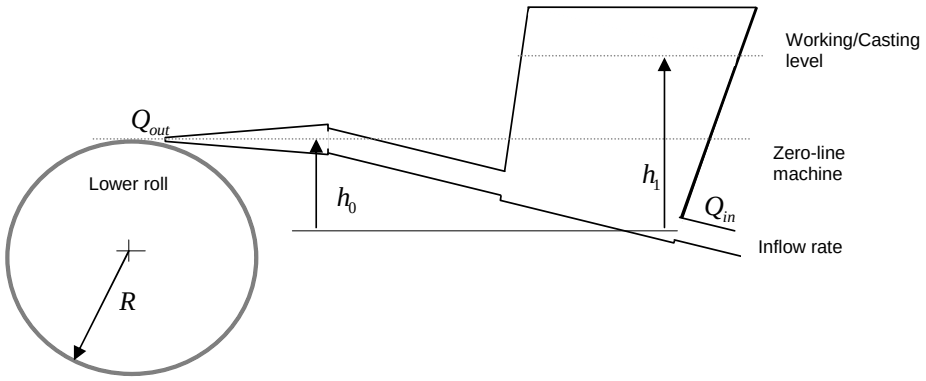

Fig. 3.3 Schematic representation of the feeding system: Head-box and the Nozzle tip aligned with the lower roll

as a controlled variable of the plant model and kept constant during the entire casting run.

Magnesium melt level in the HB is controlled to achieve a constant pressure of the melt at the nozzle tip and/or at the entrance to the rollers. For developing the mathematical model of the head-box melt level, it is assumed that the molten magnesium flow is steady, incompressible and irrotational with negligible frictional effects so the Bernoulli equation is applicable. The continuity equation of the molten metal can be described as

$$A(h)\frac{dh}{dt} = Q_{in} - Q_{out} \tag{3.1}$$

Where $h := h_1 - h_0$ and $A(h) := \frac{1}{2}\left(a_T + b_T - 2h(\tan\beta_1 + \tan\beta_2)\right)\left(d_T - h(\tan\beta_1 + \tan\beta_2)\right)$; a_T, b_T and d_T are dimensions of the head-box top surface. Variable A is the total area of the head-box which changes with the melt level as its side-walls are inclined with angles $\beta's$; h is the height of the molten metal taken relative to the nozzle tip which is adjusted to and aligned with the upper surface of the lower roll (zero-line casting machine) i.e. the axis of the nozzle is placed at the depth below the working level of the melt as shown in Fig. 3.3; Q_{in} is the control input flow rate which is regulated by control of a pump mounted on the furnace, its motor is controlled by frequency converter and Q_{out} is the output flow from the nozzle tip. According to the Daniel Bernoulli's hydrodynamics theory, the discharging velocity and volumetric flow rate out of the head-box through the nozzle are given as

$$Q_{out} = a_n c_d \sqrt{2gh} \tag{3.2}$$

Where a_n is the cross sectional area of the nozzle tip; c_d is the discharge coefficient assumed to be unity and g is the gravitational acceleration constant.

Following CANMET-MTL, suppose we need to maintain the melt level at $h_p = 0.029$ m above the zero-line casting machine and given the dimensions of the head-box a_T, b_T, d_T

and the inclined angles β_1, and β_2 as $a_T = 0.265$ m, $b_T = 0.130$ m, $d_T = 0.3481$ m, $\beta_1 = 19.5^o$, $\beta_2 = 14.4^o$, the Equation (3.1) is linearized at that melt level to yield

$$\frac{d\delta h(t)}{dt} = -0.273\delta h(t) + 16.836\delta q_{in}(t) \tag{3.3}$$

Where δh, δq_{in} are deviation variables from their operating points (i.e. $\delta h = h - h_p$ and $\delta q_{in} = q_{in} - q_{inp}$). Thus, the transfer function from inflow rate to the melt level is given by

$$G_1 = \frac{\Delta h(s)}{\Delta q_{in}(s)} = \frac{61.67}{3.663s + 1} = \frac{k_{qh}}{\tau_1 s + 1} \tag{3.4}$$

Where $\Delta h(s)$ and $\Delta q_{in}(s)$ are the Laplace transform of δh and δq_{in}, respectively.

The metal melt is forced out of the head-box through a refractory nozzle due to head pressure difference to hit cooled rotating rolls. The effect of metallostatic pressure on the solidification front position x_s is relatively small compared to the casting speed. Its dynamics, however, may be modelled as that of a first order mechanical system of spring-damper. The proposed model is essentially based on engineering intuition whereby the mushy zone (i.e. solid-liquid coexistence zone) may work as a damper and the back pressure force exerted on the melt as a result of roll hardening work may be represented as spring force. Thus, the proposed model parameters are empirically chosen so that a planar movement of the solidification front is obtained. The nozzle tip plays a vital role in determining the shape of the solidification front and due to confidentiality reasons any detail on the nozzle tip is not presented here. In short, the smooth movement of the solidification front should be guaranteed from the way the nozzle tip is designed.

The resultant exit pressure force on the nozzle that is used to excite the first order mechanical system is the product of the mass flow rate and the velocity of the melt out of the

nozzle $F_p = \dot{m}\Delta v$ where $\Delta v = v_2 - v_1 = -\sqrt{2gh}$. Thus, the approximate transfer function from the exit pressure force F_p to the solidification front position x_s is given by

$$\frac{\Delta x_s}{\Delta F_p} = \frac{1}{Bs+k} = \frac{k_{ps}}{\tau_2 s + 1}; \tau_2 = \frac{B}{k} \text{ s}; k_{ps} = \frac{1}{k} \text{ m/N} \tag{3.5}$$

Where Δx_s and ΔF_p are the Laplace transform of the solidification front position x_s and the nozzle exit pressure force F_p, respectively. The subscripts 's' and 'p' stand for solidification and pressure, respectively. B is the damper coefficient N.s/m and k is the spring constant N/m.

Since $\Delta F_p = k_{hp}\Delta h$; $k_{hp} = -2\rho g a_n$ kg.s^{-2}

Therefore

$$G_2 = \frac{\Delta x_s}{\Delta h} = \frac{k_{hp}k_{ps}}{\tau_2 s + 1} \tag{3.6}$$

The parameters B damper coefficient N.s/m and k spring constant N/m are empirically chosen such that the meniscus position is stable and therefore smooth motion of the solidification front is obtained. One possibility to identify those parameters is to assume that the transient period of the first order model is equivalent to five time constants. In order to avoid slowing down the solidification process, the transient period is assumed to be equivalent to the total solidification time given in Equation (3.8). Another effort is made to choose the spring constant k to be equivalent to the Young's modulus (modulus of elasticity) of magnesium alloy which is temperature-dependent. The Young's modulus of magnesium alloy changes from zero (at liquidus temperature) up to 35 GPa (at the mushy zone) [29]. Nevertheless, this choice was disregarded because the resulting static gain of the proposed transfer function was very large which may not represent the real dynamics. Moreover, the range of change $0 - 35$ GPa is so large that it cannot be handled as uncertainty in the

model using robust control theory.

3.2.2.3 Solidification Process

Solidification takes place at the first metal-roll contact at a solidification rate that varies along the solidification length. A uniform solidification rate, however, has to be attained. Otherwise, an uneven thickness of solidifying shells is formed during the solidification process, resulting in longitudinal surface cracks and defects due to hot deformation [13][30]. The thickness of a solidified shell can be described by the square root of time law [31][13][30]. The square root of time law is first introduced into continuous mould casting and it can be suitably generalized in twin roll casting with the assumptions that the solidification length is relatively short and the rolls are very large such that its curvature can be ignored.

$$d_{shell}(t) = \kappa\sqrt{t_s} - b \tag{3.7}$$

$$t_s = \frac{\theta_s}{\Omega_r} = \frac{L_s}{v_r} \tag{3.8}$$

Here, d_{shell} is the thickness of solidified shell mm; the gradient κ is solidification rate constant mm/min$^{0.5}$; the solidification time t_s is the time the cast strip takes to solidify to half the final strip thickness [13]; the solidification length $L_s \in (0, \ell)$ is the horizontal projection of contact area $\theta_s \in (0, \theta_0)$; v_r is the linear speed of the rotating twin rolls m/min and Ω_r is the angular velocity rad/s. The negative value of b indicates that there is a delay at the beginning of solidification, stemming from the fact that the melt casting temperature is greater than the solidification temperature by about 30^{o}C [30][13].

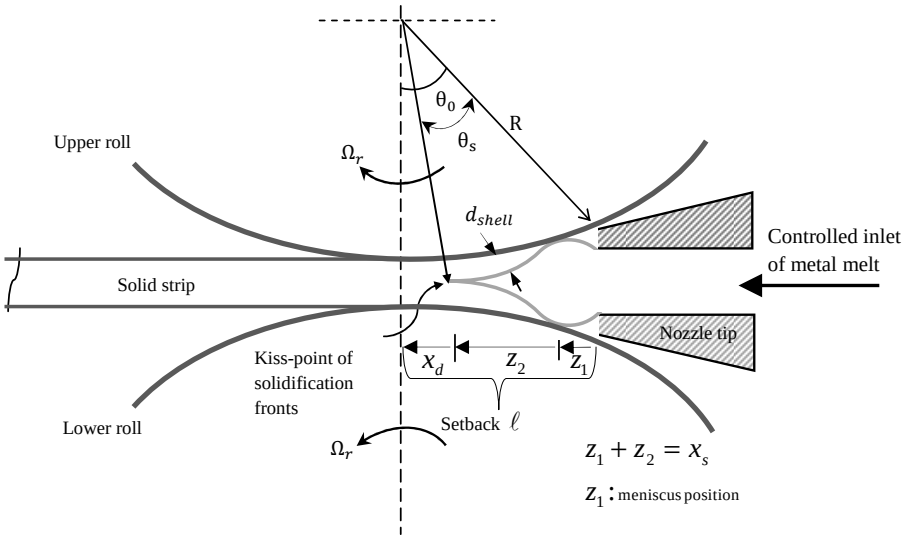

Fig. 3.4 Schematic representation of TRC

The growth constant κ can be estimated numerically by fitting data of a numerical model which is developed by a research group at the University of Waterloo. Fig. 3.5 depicts the relationship between the thickness of solidified shell and square root of solidification time. It is pertinent, however, to note that the data used in Fig. 3.5 does not take into account the change of heat transfer coefficient throughout the solidification process. A constant heat transfer coefficient of 11 kW/m^{2o}C is assumed.

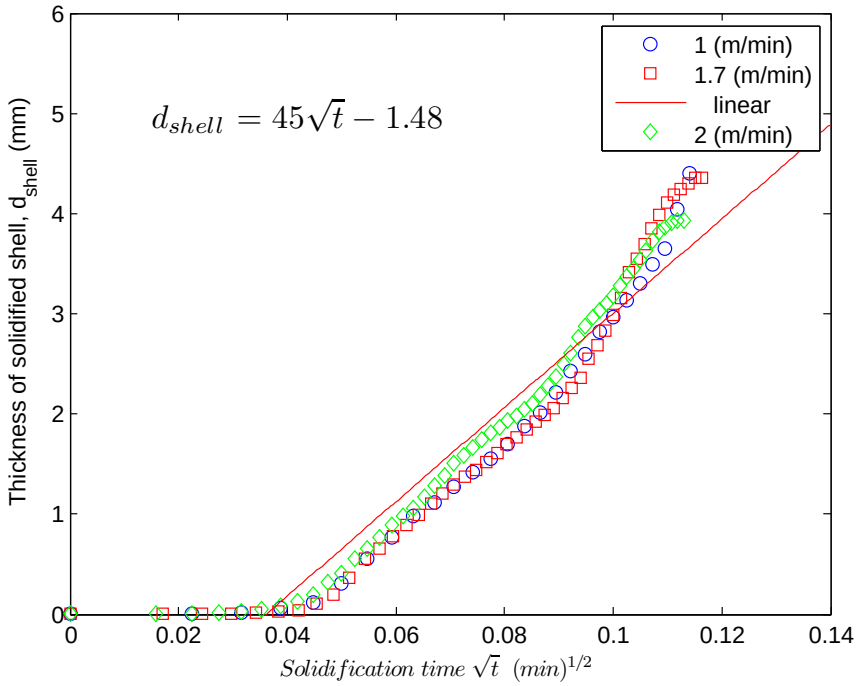

Fig. 3.5 Thickness of solidified shell as a function of square root of solidification time (*Data used to produce Fig. 3.5 is generated by a CFD simulation model, courtesy of Amir Hadadzadeh*[1])

[1]PhD Student at the University of Waterloo, working on developing a numerical model for CANMET-MTL Twin Roll Casting Process

Fig. 3.4 illustrates the following geometrical relationship that governs the solidified shell thickness at the solidification end point or "kiss-point" of solidification fronts [32], i.e., the point where the two solidified shells are bonded and/or the solidification fronts meet.

$$d_{shell}(t) = \sec\left(\theta_0 - \theta_s(t)\right) \times \left[\frac{r_g}{2} + R - R\cos(\theta_0 - \theta_s(t))\right] \tag{3.9}$$

Where r_g is the roll gap which defines the final strip thickness; R is the roll radius and θ_0 defines the set-back which refers to the distance between the nozzle tip and the rolls minimum clearance in radian.

Combining Equation (3.8) with (3.7) and equating with (3.9) yield

$$\kappa\left(\frac{\theta_s(t)}{\Omega_r}\right)^{1/2} - b = \sec\left(\theta_0 - \theta_s(t)\right) \times \left[\frac{r_g}{2} + R - R\cos(\theta_0 - \theta_s(t))\right] \tag{3.10}$$

In real practice, it is difficult to measure the position of the solidification end point (i.e. kiss-point of solidification fronts). However, the model in Equation (3.10) can be used to estimate the position of solidification fronts. More precisely, for predetermined setback, casting speed and constant exit strip thickness (i.e. constant roll gap), the nonlinear Equation (3.10) can be numerically solved for θ_s to predict the location of the "kiss-point" of solidification fronts. The analytical solution is verified using numerical simulation results, see Table 3.2. For steady production and on the basis of numerical results it has been suggested that the best ratio of the length of solidification and deformation zone $x_s : x_d$ or $\theta_s : (\theta_0 - \theta_s)$ is $1 : 3$ when the casting temperature is 700^oC [28]. If the kiss-point of solidification fronts occurs too far upstream from the nip point (kiss-point of the rolls or point of minimum clearance of the rolls), the as-cast strip can experience shrinking edges as a result of excessive roll separating force, micro-cracks and even breakdown. On the

other hand, when it is located far downstream, the as-cast strip is prone to develop re-melting marks and hot-lines as a result of low separating force [32]. Therefore, the control system must guarantee that the solidification fronts will concur within the optimum zone during casting production. The movement of solidification fronts towards the nip point is dominated by the manipulated roll casting speed. Thus, the casting speed has to be changed within an acceptable control range.

Theoretical Optimization of Processing Parameters

Linking the process parameters to strip quality may not be easy and therefore a lot of research work including real experiments has to be expended to define the optimal operating conditions and casting configurations. A major research effort is currently on-going at the CANMET-Lab by conducting real experiments and at the University of Waterloo by carrying out numerical simulations to analyze the thermal stresses in the as-cast strip for different casting parameters in order to define the optimal casting operations. However, using the aforementioned best ratio of the length of solidification and deformation zone and by dividing the deformation zone into four equal parts, the optimum position of the kiss-point of solidification fronts should lie within the optimum zone which is assumed to be the centre zone of the equally divided parts [32]. Thus, the model given in Equation (3.10) is used to calculate the acceptable control range of the linear velocity of the rotating rolls that may ensure good surface quality of the produced strip. The angular velocity Ω_r in terms of the linear seed of the rotating twin rolls is given as

$$\Omega_r = v_r/R$$

Results for different casting setting are presented in Table 3.1. Apart form the market prices of the crude materials and any other related factors, it can be seen that casting for a thinner gauge is more profitable as the production rate can be increased, but this will come at the price of the final strip quality.

Table 3.1 Theoretical optimized casting speed parameter of Magnesium TRC Machine

Casting configuration			Acceptable control range of the roll speed	
Setback ℓ mm	Reduction $\varepsilon\%$	Strip Thickness r_g mm	$v_{r\,\min}$ m/min	$v_{r\,\max}$ m/min
32.5	50	6	1.02	2.56
42.0	38	6	1.08	3.24
50.0	30	6	1.06	3.75
32.5	40	4	1.53	4.20
42.0	29	4	1.54	5.20

The maximum percent reduction $\varepsilon\%$ of solid material (i.e. maximum reduction in the exit thickness) at the roll bite can be approximated using the following Equation [14][22]

$$\varepsilon\% \simeq \frac{r_g}{r_g + \frac{\ell^2}{R}} \times 100 \tag{3.11}$$

Where ℓ is the nozzle setback in mm. As shown in Fig. 3.4, it defines the distance between the nozzle tip and the rolls minimum clearance in mm.

For a predetermined setback ℓ and other parameters remaining constant, if a step input is applied in roll angular velocity, the kiss point of solidification fronts advances toward the nip region and eventually comes to a halt after solidification time elapses. Therefore, the relationship between the solidification front position and roll angular velocity exhibits a first-order dynamical behaviour. The approximate transfer function from the rolls' angular

velocity to the position of solidification fronts is given as

$$G_3 = k_{\Omega s}\frac{1}{\tau_3 s + 1} \tag{3.12}$$

Here, the time constant τ_3, in units of s, is assumed to be equivalent to one fifth of the total solidification time over which the cast strip solidifies completely; the steady-state gain $k_{\Omega s}$, in units of m.(rad.s)$^{-1}$, is casting speed dependent and can be estimated by solving model Equation (3.10) at an operating casting speed and then at a 5% change in the operating casting speed.

3.2.2.4 Deformation Process

The amount of solid material being deformed depends on the solidification front position. When the solidified shell is formed on each surface of the rolls as a result of heat extraction, the two solidified shells bonded at the solidification end point is exerting pressure on the roll surfaces. Not only does the roll separating force affect the thickness of the produced strip but also affects the quality of the strip. Therefore, it has to be strictly controlled [33]. Now, adopting the work of Edwards [22], the roll separating force (RSF) is derived on the basis of uniform pressure distribution exerted on the roll surfaces at the nip region by integrating the pressure profile over the nip region [22].

$$F \simeq \frac{2\lambda L x_d^3}{3 r_g R} \tag{3.13}$$

where λ is the roll separating force constant (65.07×10^7 N/m^2) dependent on the plasticity of the material being rolled; x_d is deformation zone length or solidification front position in relation to the rolls centreline, as shown in Fig. 3.4; r_g is the roll gap; R is the roll radius

and L is the face length of the nozzle tip. However, the solidification front position x_s in relation to the nozzle tip at a constant nozzle setback ℓ is given as

$$x_s = \ell - x_d \tag{3.14}$$

And from the geometry given in Fig. 3.4 x_d is written

$$x_d = (R + \frac{r_g}{2}) \tan(\theta_0 - \theta_s) \tag{3.15}$$

Therefore, Equation (3.13) becomes

$$F \simeq \frac{2\lambda L(\ell - x_s)^3}{3 r_g R} \tag{3.16}$$

It can be seen from Equation (3.16) that when the kiss-point of solidification fronts moves towards the roll bite (kiss-point of the rolls), the length of deformation zone decreases, i.e. the distance $(\ell - x_s)$ decreases and therefore the roll separating force is decreased. Inversely, as the roll gap increases, the roll separating force is decreased.

Model equations (3.10) and (3.16) have been verified using numerical simulation data generated by a numerical model which is developed by Amir Haddadzadeh at the University of Waterloo. Table 3.2 illustrates that numerical model and model equations are in quit good agreement. The numerical simulation results have been found for different casting speeds, constant setback ℓ of 32.5 mm or θ_0 of 0.1841 rad, constant roll gap r_g of 6 mm and roll radius R of 177.5 mm

Table 3.2 Comparison between model equations (3.10) & (3.16) and Amir Haddadzadeh's numerical model

Casting speed	Model equations		Numerical model		% of error	
v_r m/min	x_s mm	F kN	x_s mm	F kN	in x_s	in F
1.0	13.98	646.0	10.68	567	30.9	13.93
1.7	19.90	203.0	19.37	190	2.73	6.84
2.0	22.16	112.5	22.93	107	3.36	5.14
2.5	26.00	30.00	28.93	35	10.13	14.28

There are slight discrepancies resulting from considering constant solidification rate κ mm/min$^{0.5}$ throughout the solidification process.

Since both solidification and deformation processes takes only a fraction of a second, it is sufficient to find the steady-state relationship, in units of N/m, of roll separating force with the solidification front position by linearizing Equation (3.16) around a small region for constant setback and roll gap.

$$\delta F = -k_{sf}\delta x_s \tag{3.17}$$

Remark 1: The negative sign in front of $k_{sf} \in \mathbb{R}^+$ may have a physical meaning that as the solidification front position advances toward the roll bite, the roll separating force decreases. However, it may be excluded from the model without jeopardizing the dynamic representation of the roll separating force as it results a positive closed loop feedback and therefore negative control gains are required. More importantly, neither the roll separating force nor the solidification front position has to be negative.

Taking the Laplace transform of Equation (3.17) yields

$$G_4 = \frac{\Delta F}{\Delta x_s} = k_{sf} \tag{3.18}$$

Thus, the linear dynamical model of CANMET-MTL Twin Roll Casting machine (TRC), shown in Fig. 3.6, is given as

$$\Delta\mathbf{Y}(s) = \mathbf{G}(s)\Delta\mathbf{U}(s)$$

$$\Delta\mathbf{Y} \in \mathbb{C}^2, \mathbf{G} \in \mathbb{C}^{2\times 2}, \text{and } \Delta\mathbf{U} \in \mathbb{C}^2$$

with

$$\Delta\mathbf{Y}(s) = \begin{bmatrix} \Delta F(s) \\ \Delta h(s) \end{bmatrix}; \Delta\mathbf{U}(s) = \begin{bmatrix} \Delta\Omega_r(s) \\ \Delta q_{in}(s) \end{bmatrix}$$

and the 2×2 transfer function matrix (TFM)

$$\mathbf{G}(s) = \begin{bmatrix} k_{\Omega s}k_{sf}\dfrac{1}{\tau_3 s+1} & \dfrac{k_{qh}}{\tau_1 s+1}\dfrac{k_{hp}k_{ps}}{\tau_2 s+1}k_{sf} \\ 0 & \dfrac{k_{qh}}{\tau_1 s+1} \end{bmatrix} \tag{3.19}$$

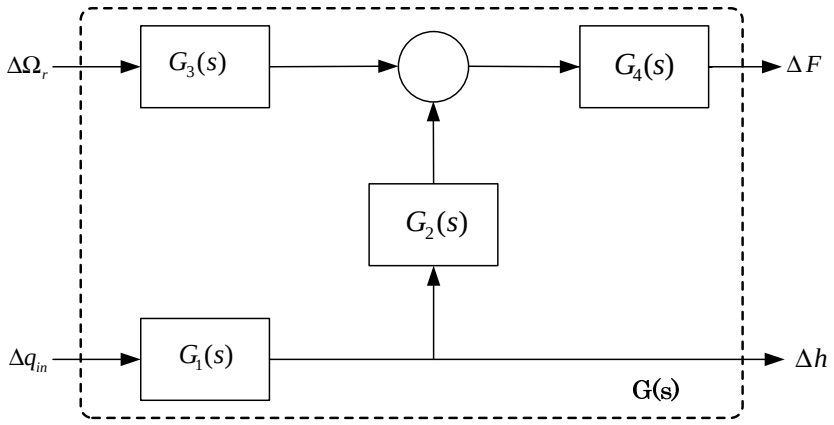

Fig. 3.6 Linear multivariable dynamic model of TRC

Remark 2: The above formulated model does not incorporate the dynamics of the actuators (melt pump and rotating roll drives). Loosely speaking, actuators could have fixed frequency response over a much broader frequency band than the transfer function of the

plant model. In that sense, the actuator dynamics may be neglected and assumed to have unity transfer function.

It is pertinent to note that time constants τ_2, τ_3 and static gains are casting speed-dependent (i.e., plant dynamics change with the operating conditions). Yet again, time constants τ_2 and τ_3 are assumed to be equivalent to one fifth of the solidification time which is a function of the casting speed, see Equation (3.8). The assumption is made based on the fact that transient time response of a first-order system takes only five time constants. The settling time is assumed to be equivalent to the solidification time.

$$t_s = 5\tau_2 = 5\tau_3$$

Where t_s is computed from Equation (3.8) for predetermined casting speed and θ_s is obtained by solving Equation (3.10) numerically.

Similarly, steady state gains $k_{\Omega s}$ and k_{sf} are changing with casting speed because as the casting speed ramps up, the solidification front position (θ_s in rad and x_s in mm) increases and deformation length ($\theta_0 - \theta_s$ in rad and x_d in mm) decreases, resulting in a minor change in the metallostatic pressure on solidification fronts. k_{sf} is obtained as a result of linearization of Equation (3.16) around an operating casting speed which gives the operating value of x_s and $k_{\Omega s}$ is identified by collecting data from Equation (3.10); first solving Equation (3.10) for predetermined operating casting speed and then for small perturbation, say 5%, of the predetermined operating casting speed.

$$k_{\Omega s} = \frac{\Delta x_s}{\Delta \Omega_r}$$

From Table 3.1, the casting configuration is chosen such that a reduction of 50% in strip

thickness (6 mm) is obtained (i.e. $\ell = 32.5$ mm) and an operating casting speed of 2 m/min (0.1878 rad/s) is also chosen for nominal operation. Therefore, the nominal transfer function matrix of the linear dynamical model becomes

$$\mathbf{G}(s) = \begin{bmatrix} \dfrac{2567}{0.135\text{s} + 1} & \dfrac{\text{- } 5.643 \times 10^5}{(3.663\ \text{s} + 1)\,(0.135\ \text{s} + 1)} \\ 0 & \dfrac{61.67}{3.663\ \text{s} + 1} \end{bmatrix} \tag{3.20}$$

The above transfer function matrix is converted to a state-space model of the form

$$\frac{d}{dt}\mathbf{x}(t) = \mathbf{A}\mathbf{x}(t) + \mathbf{B}\mathbf{u}(t), \quad \mathbf{y}(t) = \mathbf{C}\mathbf{x}(t)$$

with real valued matrices $\mathbf{A} \in \mathbb{R}^{4\times4}$, $\mathbf{B} \in \mathbb{R}^{4\times2}$, $\mathbf{C} \in \mathbb{R}^{2\times4}$, which are given as

$$\mathbf{A} = \begin{bmatrix} & x_1 & x_2 & x_3 & x_4 \\ x_1 & -0.2390 & 0.4958 & 0.0002 & 0.0000 \\ x_2 & -0.4916 & -7.4414 & -0.0024 & -0.0000 \\ x_3 & -0.0001 & -0.0000 & -0.2730 & 0.0058 \\ x_4 & 0.1807 & 0.0125 & 0.0058 & -7.4074 \end{bmatrix}$$

$$\mathbf{B} = 10^3\times \begin{bmatrix} & u_1 & u_2 \\ x_1 & 0.0032 & -0.3675 \\ x_2 & -0.0467 & -0.3660 \\ x_3 & 0.0008 & -0.0001 \\ x_4 & -1.0156 & 0.1300 \end{bmatrix}$$

$$\mathbf{C} = \begin{bmatrix} & x_1 & x_2 & x_3 & x_4 \\ y_1 & 367.5371 & -369.0187 & -0.0630 & -0.0001 \\ y_2 & -0.0429 & -0.0030 & 538.7494 & 0.4350 \end{bmatrix}$$

$$\mathbf{D} = \begin{bmatrix} & u_1 & u_2 \\ y_1 & 0 & 0 \\ y_2 & 0 & 0 \end{bmatrix}$$

Converting the transfer function matrix does not always give the minimal state space realizations. In order to find the minimal state space realizations, we convert the transfer function models $G_1(s)$, $G_2(s)$, $G_3(s)$ as shown in Fig. 3.6 to state space rather than combining them in the TFM $\mathbf{G}(s)$ and then converting the TFM to state space form. Thus, the minimal state space form is given as

$$\mathbf{A} = \begin{bmatrix} & x_1 & x_2 & x_3 \\ x_1 & -7.407 & 0 & 8.418 \\ x_2 & 0 & -7.407 & 0 \\ x_3 & 0 & 0 & -0.273 \end{bmatrix}$$

$$\mathbf{B} = \begin{bmatrix} & u_1 & u_2 \\ x_1 & 0 & 0 \\ x_2 & 1 & 0 \\ x_3 & 0 & 4 \end{bmatrix}$$

$$\mathbf{C} = \begin{bmatrix} & x_1 & x_2 & x_3 \\ y_1 & -3.285 \times 10^4 & 1.843 \times 10^4 & 0 \\ y_2 & 0 & 0 & 4.209 \end{bmatrix}$$

$$\mathbf{D} = \begin{bmatrix} & u_1 & u_2 \\ y_1 & 0 & 0 \\ y_2 & 0 & 0 \end{bmatrix}$$

3.3 Summary

In this chapter, a linear multivariable dynamic model of the twin roll caster at CANMET-MTL is formulated for control synthesis. A simple 2×2 transfer function matrix is obtained. The manipulated variables of the plant are volumetric inflow rate of the molten metal Q_{in} and the angular velocity of the rolls Ω_r whereas the corresponding output variables are the melt level in the head-box h taken relative to the zero-line machine h_0 and the roll separating force F. For this end, the obtained 2×2 transfer function matrix is admittedly a crude model of the CANMET-MTL TRC machine, and yet it is simple and captures important dynamical features of the plant. An acceptable control range of casting speeds is obtained for different casting configurations. It is pertinent, however, to note that casting speed is somehow related to the strip quality (strip with clean surfaces; free of defects, cracks, remelting points and hot lines) and finding the optimal range of casting speeds is an ongoing research area at CANMET-MTL laboratory. Further research on the effects of casting speed on the solidification front position, roll separating force and the effects of those parameters on the strip quality can lead to more accurate model. Furthermore, no explicit expression has been found for solidification front position (kiss-point position of solidification fronts) which can improve the accuracy of the model.

Chapter 4

Analysis and Control

This chapter is concerned with analysing the dynamics of CANMET-MTL twin roll casting machine that were modelled as a simple 2×2 transfer function matrix (TFM) in the previous chapter. Broadly speaking, a multi-input multi-output (MIMO) system is characterized by a TFM compared with a single input single output (SISO) system which is represented by a single transfer function. In this study, the CANMET-MTL strip casting machine has been represented by a 2×2 TFM (i.e. there are 4 transfer functions). The resulting TFM, which is a square matrix, is used to study the multivariable characteristics of the CANMET-MTL strip casting machine. In carrying out the analysis, an appropriate scaling of the actual plant model is selected and the amount of interaction is determined by obtaining the relative gain array (RGA) at steady state. Moreover, in order to give insight into the characteristics of such a multi-input multi-output system (MTMO), the multivariable poles and zeros will be obtained. In view of the analysis carried, an adequate control structure is proposed and suitable controllers are designed such that the process of interest is stable and the nominal performance is preserved. Multivariable (centralized) optimal controller to attain nominal performance is designed for CANMET-MTL strip casting machine using

$\mathcal{H}_\infty$ synthesis. Also, simulation results are presented

4.1 Analysis

4.1.1 Mutlivariable Poles and Zeros

The positions of poles and zeros, by definition, provide valuable information of the system dynamics relevant to the plant performance limitations and controller design . The zeros z_i of MIMO linear time invariant systems are defined as the values of s at which the transfer function matrix $\mathbf{H}(s)$ loses rank (i.e. determinant of $\mathbf{H}(s)|_{s=z_i} = 0$) whereas the poles p_i are defined as the roots of the denominator polynomials of each element of the transfer function matrix, but this method does not give information on the multiplicity of the poles. The multiplicity of the poles can be found by computing the determinant of the TFM, $\mathbf{H}(s)$ if the TFM is square (# of inputs equals to # of outputs). Nevertheless, Smith-McMillan transformation is the most effective computation method to obtain the multivariable poles and zeros [34].

4.1.1.1 Smith-McMillan Form

Definition [1]: Given a rational transfer function matrix $\mathbf{H}(s)$. There exist unimodular polynomial matrices $\mathbf{U}(s)$ and $\mathbf{V}(s)$ such that:

$$\mathbf{H}(s) := \mathbf{U}(s)\mathbf{M}(s)\mathbf{V}(s)$$

[1] Definitions and notions are borrowed from [34]

Where $\mathbf{M}(s)$ is the Smith-McMillan transformation of $\mathbf{H}(s)$ given by

$$\mathbf{M}(s) := \begin{bmatrix} \frac{\varepsilon_1(s)}{\psi_1(s)} & 0 & 0 & 0 & 0 & 0 \\ 0 & \frac{\varepsilon_2(s)}{\psi_2(s)} & 0 & 0 & 0 & 0 \\ 0 & 0 & . & 0 & 0 & 0 \\ 0 & 0 & 0 & . & 0 & 0 \\ 0 & 0 & 0 & 0 & \frac{\varepsilon_p(s)}{\psi_p(s)} & 0 \\ 0 & 0 & 0 & 0 & 0 & 0 \end{bmatrix}$$

- The zeros of the transfer function matrix $\mathbf{H}(s)$ are the roots of $\varepsilon_i(s)$, $i = 1, ..., p$
- The poles of the transfer function matrix $\mathbf{H}(s)$ are the roots of $\psi_i(s)$, $i = 1, ..., p$

where $\{\psi_i(s), \varepsilon_i(s)\}$ are coprime, $i = 1, ..., p$ and p is the normal rank of $\mathbf{H}(s)$

Poles and Zeros of CANMET-MTL Strip Casting Machine

Multivariable poles and zeros of the CANMET-MTL TRC machine, which is modelled as a simple 2×2 TFM given in Equation (3.20), can be obtained through Smith-McMillan transformation. The MIMO MATLAB^{TM} Toolbox provides a function called *smform* to compute the poles, zeros and Smith-McMillan form [34]. Thus, using *smform*, the linearized dynamics of the CANMET-MTL strip casting machine has 3 stable poles and one left half plane (LHP) zero that are located at $p_1 = -0.273$, $p_{2,3} = -7.407$ and $z_1 = -0.273$. It is pertinent to note that pole/zero cancellation is not possible in MIMO systems in which each pole and zero is associated with a different direction. Generally speaking, directionality is an interesting property of MIMO systems which can be quantified using the singular value decomposition of TFM [35].

Since all the poles and zeros are in the left half plane, the linearized dynamics of the

CANMET-MTL strip casting machine are stable and minimum phase. Therefore, tight control design is theoretically possible using decentralized control technique [36].

4.1.2 Scaling

The mathematical model derived in Chapter 3 is obtained in terms of the deviation variables. The plant model can be obtained in terms of the scaled variables so as to render the plant model analysis and controller design much simpler [35]. In general, scaling is used when there is inconsistency in the physical dimensions of input and output signals in order to make them comparable and less than 1 in magnitude. It can also be used to characterize the physical constraints of signals such as actuator saturation. The simplest approach of scaling (rough scaling) is dividing each (deviation) variable by its maximum allowed change. A more complicated approach is using weighting functions as we will see later in $\mathcal{H}_\infty$ control problem. In the latter approach, weight selection is actually a scaling problem [37] over a frequency band (frequency-dependent weighting function) compared to the former approach which is independent of frequency. For typical 2×2 plant, an appropriate scaling is shown in Fig. 4.1.

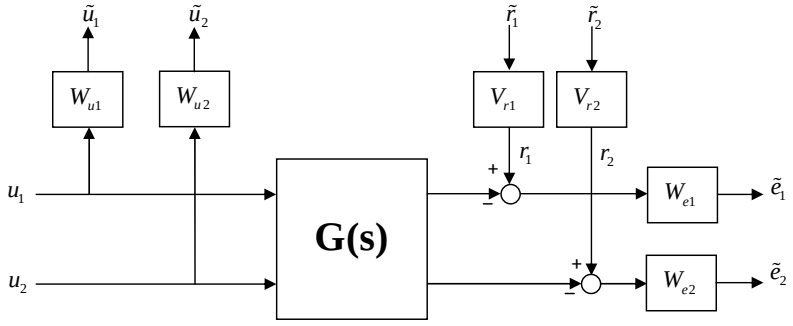

Fig. 4.1 Scaling of a $2 \times 2-$ plant

From the figure above, the scaled tracking error $\tilde{e}$ in terms of the scaled reference $\tilde{r}$ and

the scaled control signal $\tilde{u}$ is given by [37]

$$\tilde{e} = W_e V_r \tilde{r} - W_e G W_u^{-1} \tilde{u} \tag{4.1}$$

where the scaled plant $\tilde{G} = W_e G W_u^{-1}$

In this application, the CANMET-MTL TRC has inputs and outputs of different physical dimensions: inflow rate of m^3/s, roll casting speed of rad/s, roll separating force of kN and melt level of m. In Chapter 3, an allowed change of the casting speed for predetermined casting configuration is obtained, see table 3.1. The maximum allowed change of the casting speed is 2.56 m/min (0.2404 rad/s). Accordingly, the maximum allowed change (worst-case value) of the roll separating force is 30 kN. For melt level and inflow rate, the maximum allowed changes are assumed to be 0.029 m and 0.000943 m^3/s respectively. Therefore, an internal (rough) scaling of the plant $\mathbf{G}(s)$ is obtained by dividing each deviation variable by its maximum expected change.

$$\begin{bmatrix} \Delta F \\ \Delta h \end{bmatrix} = \begin{bmatrix} g_{11}(s) & g_{12}(s) \\ g_{21}(s) & g_{22}(s) \end{bmatrix} \begin{bmatrix} \Delta\Omega_r \\ \Delta q_{in} \end{bmatrix}$$

$$\begin{bmatrix} \tilde{F} \\ \tilde{h} \end{bmatrix} = \underbrace{\begin{bmatrix} 1/F_{\max} & 0 \\ 0 & 1/h_{\max} \end{bmatrix} \begin{bmatrix} g_{11}(s) & g_{12}(s) \\ g_{21}(s) & g_{22}(s) \end{bmatrix} \begin{bmatrix} \Omega_{r\max} & 0 \\ 0 & q_{in\max} \end{bmatrix}}_{\tilde{\mathbf{G}}(s)} \begin{bmatrix} \tilde{\Omega}_r \\ \tilde{q}_{in} \end{bmatrix}$$

with scaled variables $\tilde{F} = \frac{\Delta F}{F_{\max}}$, $\tilde{h} = \frac{\Delta h}{h_{\max}}$, $\tilde{\Omega}_r = \frac{\Delta\Omega_r}{\Omega_{r\max}}$, and $\tilde{q}_{in} = \frac{\Delta q_{in}}{q_{in\max}}$.

Thus,

$$\tilde{\mathbf{G}}(s) = \begin{bmatrix} \frac{20}{(0.135s+1)} & \frac{-17.2}{(0.135s+1)(3.663s+1)} \\ 0 & \frac{2}{(3.663s+1)} \end{bmatrix}$$

It can easily be seen that performing control analysis with the scaled plant model $\tilde{\mathbf{G}}(s)$ would be much simpler than with the actual plant model (i.e. model in terms of deviation variables) given in the previous chapter, Equation (3.20) because the scaled plant model has smaller gains. It is pertinent to note however that the characteristics of the actual plant model are preserved by scaling except for directionality property which is affected by scaling because of scaling-dependent singular values and condition number.

4.1.3 Stability of a MIMO System

The Nyquist stability criterion of SISO systems can be generalised to MIMO systems. **Theorem** [2]: "*If* $\mathbf{G}(s)$ *has right half plane poles (RHPP), p, given by the Smith-McMillan transformation, then the closed loop with negative feedback is stable if and only if the characteristic graphs of* $\mathbf{KG}(s)$ *surround the point (-1,0) p times in a counterclockwise direction, assuming that there was no cancellations of instabilities*".

Letting $\mathbf{K} = kI; \quad k \in \mathbb{R}$. Fig. 4.2 illustrates the generalized Nyquist diagram of the transfer function matrix $\tilde{\mathbf{G}}(s)$ when $k = 1$ which confirms the above statement on stability; the plant model $\mathbf{G}(s)$ is stable and minimum phase, since the number of surroundings of the characteristic graphs around $(-1, 0)$ is equal to zero.

[2] Theorem statement is borrowed from [34]

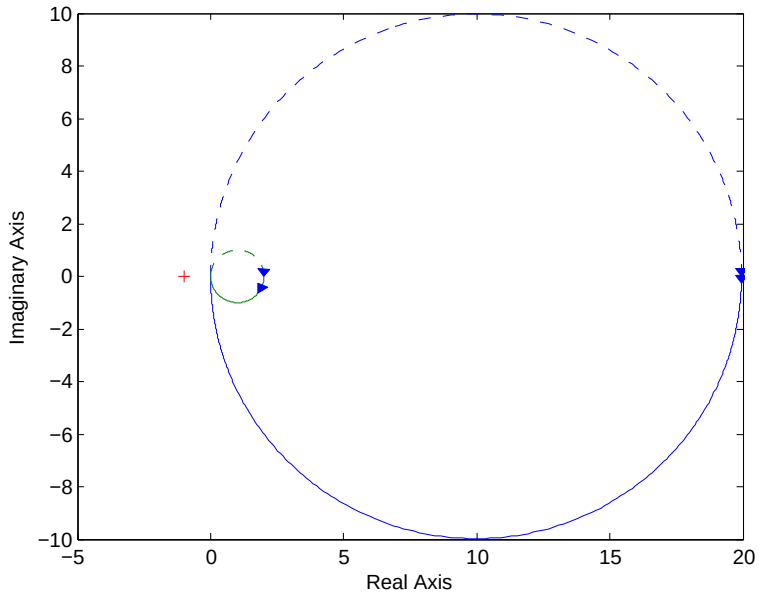

Fig. 4.2 General Nyquist diagram of the 2×2 scaled plant

4.1.4 Relative Gain Array (RGA)

In most cases, a control problem is reduced to a single-input single-output (SISO) control problem where a single input (manipulated variable) is related to a single output (controlled variable) via simple transfer function and any other exogenous variable imposed on the SISO control loop is treated as a disturbance. With MIMO systems, however, the exogenous variables imposed on a SISO control loop are taken into account as interaction (referred to as a coupling, i.e. manipulation of any input affects all outputs). In the literature, there are several useful tools that can be used to quantify the degree of coupling or interaction among different control loops. For example, the Nyquist's arrays and the Gershgorin bands, the relative gain array (RGA) and individual channel analysis and design (ICAD). The RGA provides a useful tool to quantify the amount of interaction in MIMO systems while the aforementioned directionality is quantified by the condition number which is defined as the

ratio of the maximum singular value to the minimum singular value [35]. The RGA-based analysis suggests how the input-output pairings should be chosen. In general, the rule of thumb of input-output pairings is to pair inputs and outputs such that the diagonal elements of the RGA are large and positive. The traditional pairing based on which the CANMET-MTL TRC plant model has been formulated is a diagonal pairing (i.e. $(\Omega_r,\ F)$ and $(q_{in},\ h)$). This traditional pairing is investigated by RGA-based analysis. Nonetheless, it might be this is the only present choice for this application because the transfer function matrix of the CANMET-MTL TRC model is a triangular. However, it would be of interest to see how RGA-based analysis is performed for a $2\times2-$ plant model. One of the interesting properties of the RGA measure is that it is not scaling dependent. Thus, the RGA analysis is performed on the scaled plant model.

The RGA for a square plant is defined by

$$\Lambda(\mathbf{G}(s)) \triangleq \mathbf{G}(s).*(\mathbf{G}(s)^{-1})^T$$

where Λ is the RGA of the transfer function matrix $\mathbf{G}(s)$, the operator $.*$ denotes element-wise multiplication.

For a 2×2 plant, a symmetric RGA matrix is obtained:

$$\Lambda = \begin{pmatrix} \lambda_{11} & \lambda_{12} \\ \lambda_{21} & \lambda_{22} \end{pmatrix} = \begin{pmatrix} \lambda_{11} & 1-\lambda_{11} \\ 1-\lambda_{11} & \lambda_{11} \end{pmatrix}$$

For steady-state ($s = 0$), each element in the RGA is defined as the open-loop gain divided by the gain between the same variables when the other loops are controlled, i.e. $\lambda_{ij} = \frac{(\partial y_i/\partial u_i)_{u_{k\neq j}}}{(\partial y_i/\partial u_j)_{y_{k\neq i}}},\ i,j = 1,2$

The steady state-RGA of the 2×2 scaled plant $\tilde{\mathbf{G}}(s)$ is computed using MATLAB^{TM}

implemented function called *rga* $\Lambda = \begin{pmatrix} 1 & 0 \\ 0 & 1 \end{pmatrix}$

Thus, the diagonal elements of the RGA are unity, indicating the decentralized control could be considered with pairings ($\Omega_r - F$) and ($q_{in} - h$).

4.2 Control Objectives

Broadly speaking, the key objective of a control system is to make the plant (process) outputs behave in a desired manner by manipulating the plant inputs. In this application, the control objectives are to maintain stability and nominal performance by manipulating the plant inputs. In plain words, the control objectives are to maintain the roll separating force constant and require the head-box melt level to reach a set point by manipulating roll casting speed and melt inflow rate respectively. Controlling the roll separating force is of paramount importance to strip quality and strip thickness. Regarding strip quality, high roll separating force improves heat transfer between roll surfaces and the as-cast strip. However, the higher the roll separating force the greater the likelihood that the as-cast strip will experience surface cracks, defects and hot-lines. Regarding strip thickness, the strip thickness is strongly coupled with roll separating force and initial roll gap. The coupling relationship is given by the following Equation [3].

$$d = r_g + \frac{F}{M}$$

where d is the final strip thickness, F is the roll separating force and M is the mill modulus. Start up operation, which involves very complex dynamics, is assumed to be stable.

[3] gauge-meter equation

4.3 Controller Design

The aim of this section is to synthesize a controller for the CANMET-MTL TRC model. First, a classic control design is carried out in order to compare the results with $\mathcal{H}_\infty$-optimal control. The drawbacks of each method are illustrated.

4.3.1 Decentralized Feedback Control (classic control)

Decentralized feedback control system consists of independent subsystems (SISO). In practice, decentralized control is widely used for multivariable plants due to several advantages [38]:

- Saving on modelling effort compared with multivariable control which requires complex and good plant models.
- Flexibility in operation and failure tolerance. For example, It is easy for operators to bring a subsystem in and out of service for maintenance purposes, if an actuator or sensor fails, with no change on the other subsystems.
- Controller parameters are easy to tune and even retune on-line to accommodate the changes of process conditions.

The problem of decentralized feedback control is to design a diagonal controller that achieves good control performance on a square plant $\mathbf{G}(s)$. Fig. 4.3 depicts the decentralized feedback control problem for 2×2 plant. Authors like Zames and Bensoussan [39] proved that good control performance can be achieved with decentralized feedback control as long as the controlled plant is stable and has no RHP zeros that may impose performance limitations. Moreover, good steady-state performance is achievable if and only if $\mathbf{G}(s)|_{s=0}$ is non-singular [38].

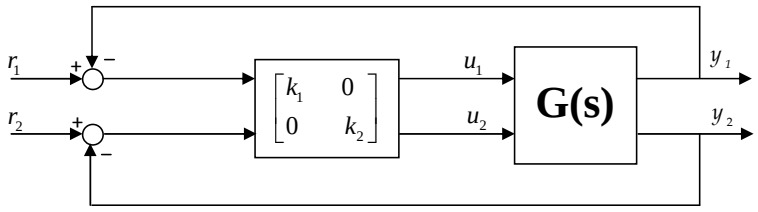

Fig. 4.3 Decentralized (diagonal) feedback control of a 2×2 plant

In general, decentralized feedback control design requires two steps: First, interaction assessment based on which the best pairing is selected. Second, designing and tuning a controller for each control loop independently [35].

4.3.1.1 Design and Simulation Results

In this subsection we present simulation results illustrating the performance of the decentralized feedback control designed for a simplified multivariable dynamic model of CANMET-MTL TRC machine. Proportional-Integral (PI) decentralized controller of the form

$$\begin{bmatrix} k_{p1} + \frac{k_{I1}}{s} & 0 \\ 0 & k_{p2} + \frac{k_{I2}}{s} \end{bmatrix}$$

is proposed and manually tuned using a trial-and-error method. Fig. 4.4 shows the SIMULINK model of the CANMET-MTL TRC machine with the PI-decentralized controller. From the foregoing discussion and analysis, the CANMET-MTL TRC machine, modelled by simple 2×2 triangular transfer function matrix, is stable and minimum phase system and as for interaction assessment, despite the fact that the plant model is partly interacting (i.e. the melt level in the head-box is not affected by the casting speed because the nozzle tip, which is distant from the rolls by 0.2 mm, uniformly distributes the metal

along across the width of the rolls and the gap between the rolls does not work as a mass storage), the RGA matrix indicates that the pairing $F - \ \Omega_r$ and $h - \ q_{in}$ is appropriate. Therefore, it is expected that the proposed PI- diagonal controller achieve good control performance.

Proportional-Integral (PI) controllers are designed and independently tuned for each con-

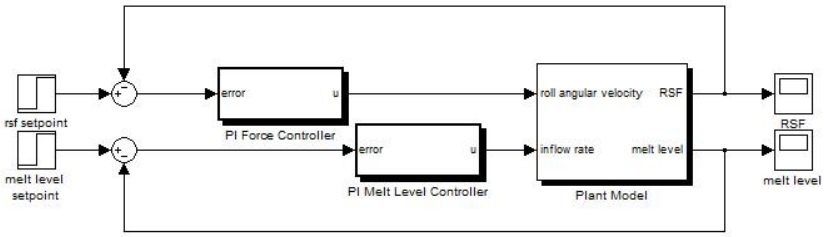

Fig. 4.4 SIMULINK block diagram of the PI-decentralized feedback control of CANMET-MTL TRC

trol loop. For the roll separating force control loop, the RSF is kept constant at the nominal value of 112.5 kN using a PI controller with tuning gains of $k_{p1} = 0.15$ and $k_{I1} = 15$. As for the melt level control loop, good reference tracking is achieved by a PI controller with tuning gains of $k_{p2} = 0.8$ and $k_{I2} = 0.2$. The control signal plots and the step responses of the linear controlled plant model with different tuning gains of the controllers are shown in Fig. 4.5. The relative step responses for the desired performance are shown in Fig. 4.6. As we expected, decentralized feedback control provides good performance for this stable plant with moderate controller gains.

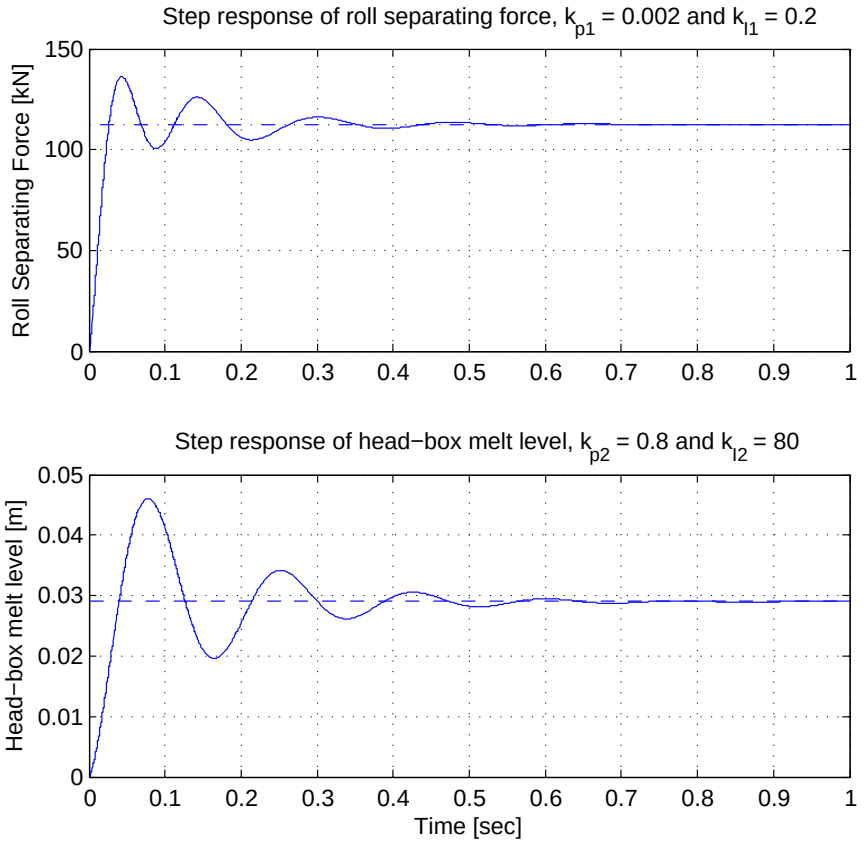
Step response of roll separating force, k_{p1} = 0.002 and k_{I1} = 0.2
Roll Separating Force [kN]
150
100
50
0
0 0.1 0.2 0.3 0.4 0.5 0.6 0.7 0.8 0.9 1
Step response of head−box melt level, k_{p2} = 0.8 and k_{I2} = 80
Head−box melt level [m]
0.05
0.04
0.03
0.02
0.01
0
0 0.1 0.2 0.3 0.4 0.5 0.6 0.7 0.8 0.9 1
Time [sec]

(a)

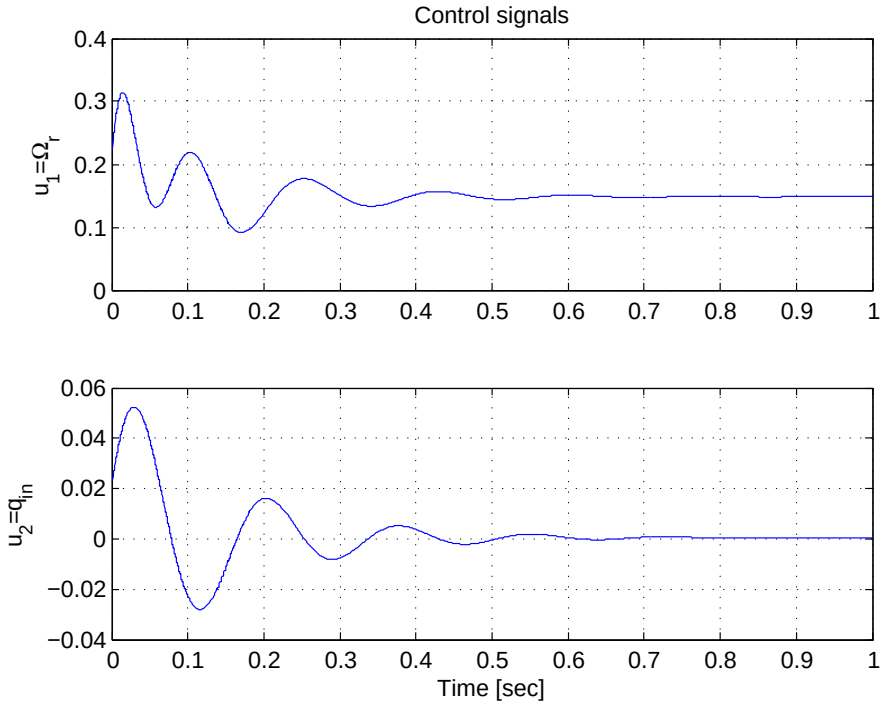
Control signals
$u_1=\Omega_r$
0.4
0.3
0.2
0.1
0
0 0.1 0.2 0.3 0.4 0.5 0.6 0.7 0.8 0.9 1
$u_2=q_{in}$
0.06
0.04
0.02
0
−0.02
−0.04
0 0.1 0.2 0.3 0.4 0.5 0.6 0.7 0.8 0.9 1
Time [sec]

(b)

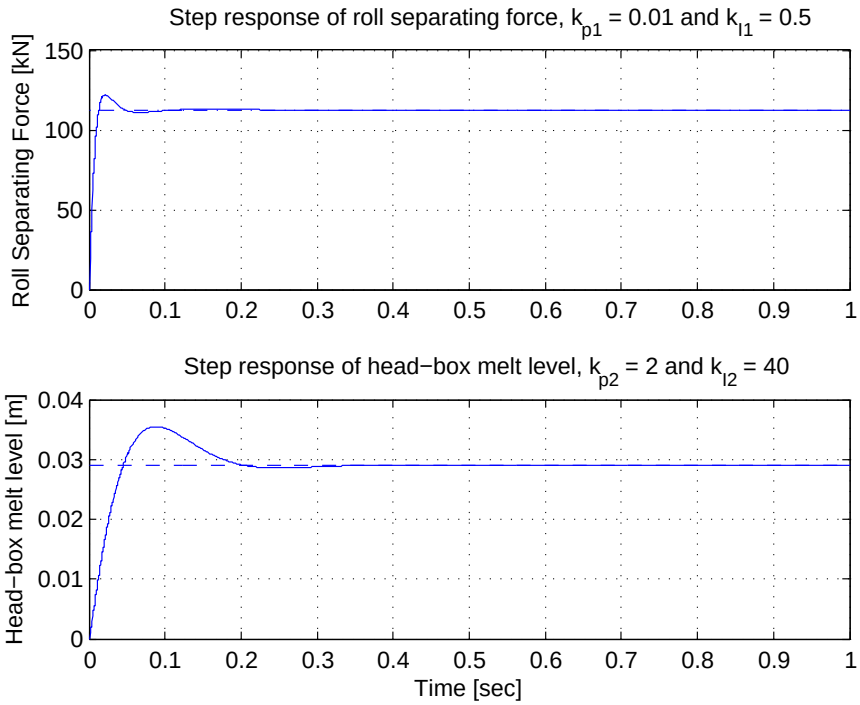
Step response of roll separating force, k_p1 = 0.01 and k_I1 = 0.5
Roll Separating Force [kN]
150
100
50
0
0 0.1 0.2 0.3 0.4 0.5 0.6 0.7 0.8 0.9 1
Step response of head−box melt level, k_p2 = 2 and k_I2 = 40
Head−box melt level [m]
0.04
0.03
0.02
0.01
0
0 0.1 0.2 0.3 0.4 0.5 0.6 0.7 0.8 0.9 1
Time [sec]

(c)

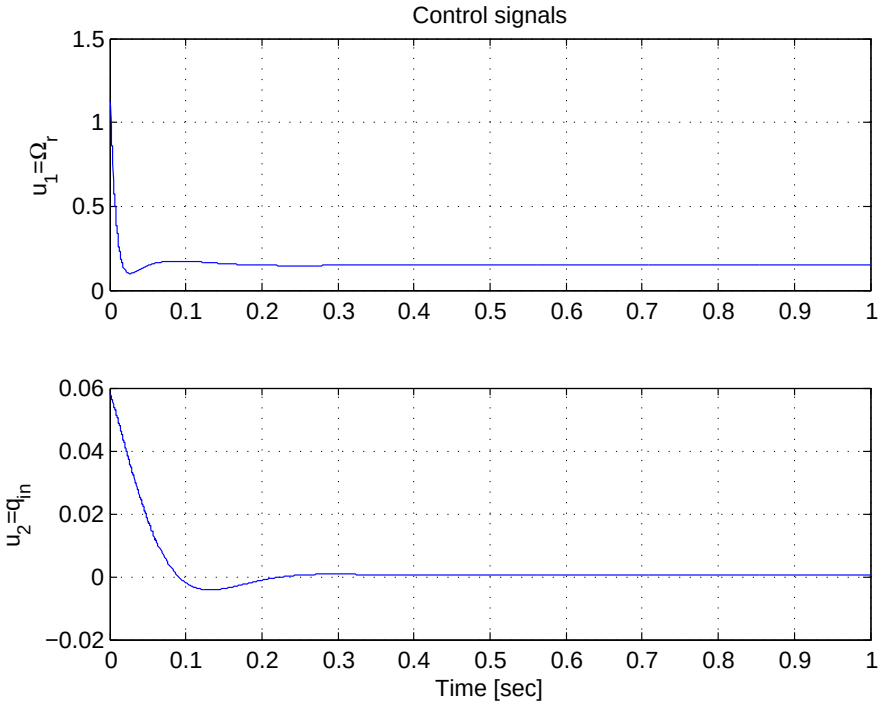
Control signals
u_1=Ω_r
1.5
1
0.5
0
0 0.1 0.2 0.3 0.4 0.5 0.6 0.7 0.8 0.9 1
u_2=q_in
0.06
0.04
0.02
0
−0.02
0 0.1 0.2 0.3 0.4 0.5 0.6 0.7 0.8 0.9 1
Time [sec]

(d)

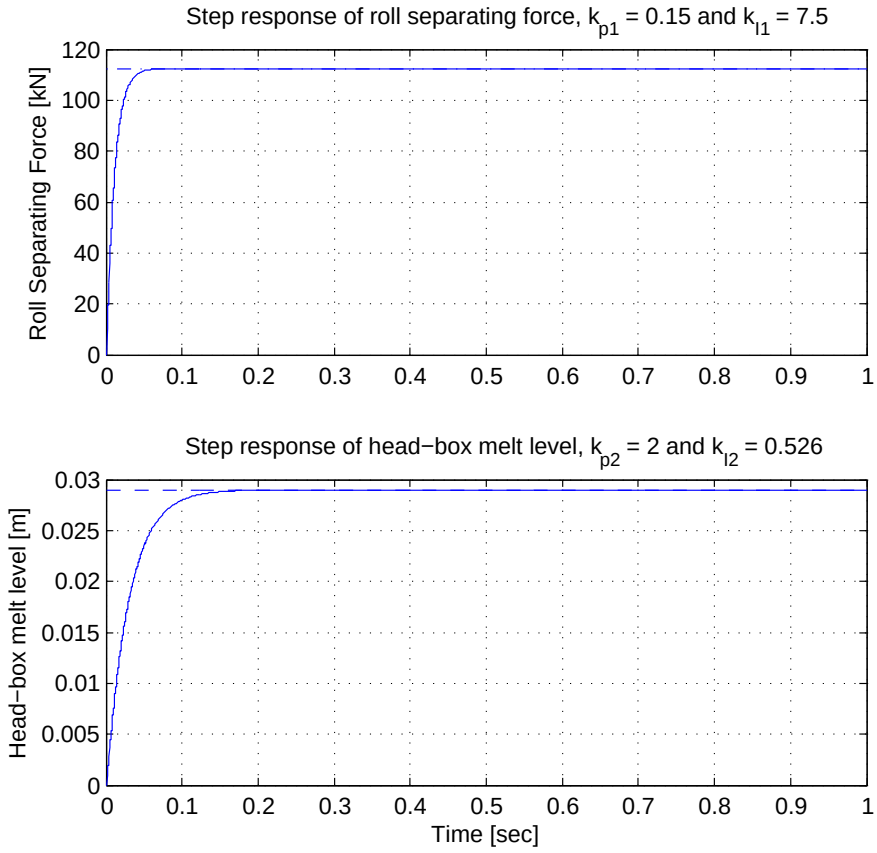

(e)

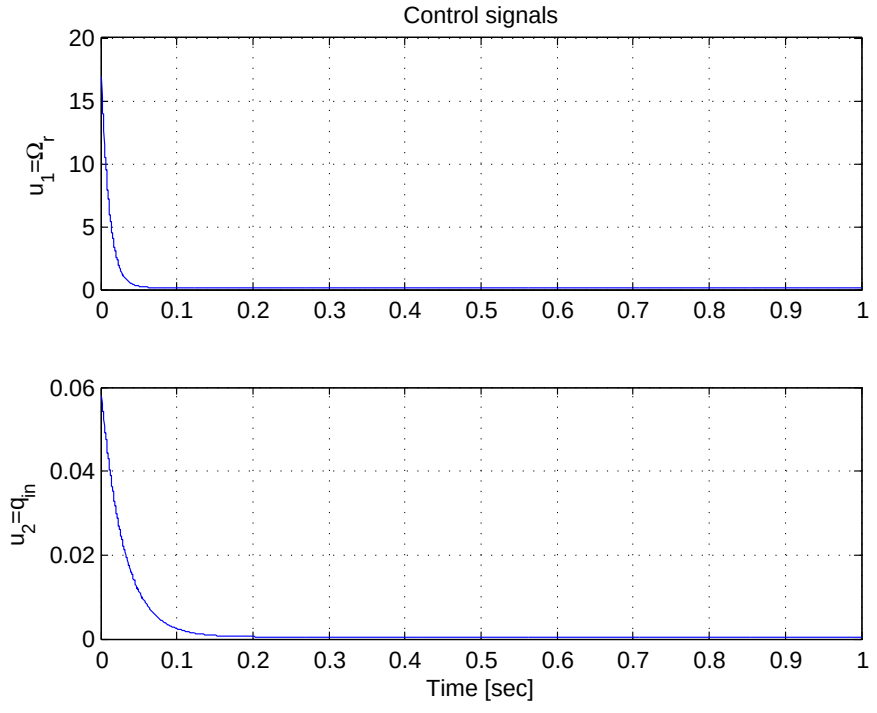

(f)

Fig. 4.5 Reference step responses and control signal plots

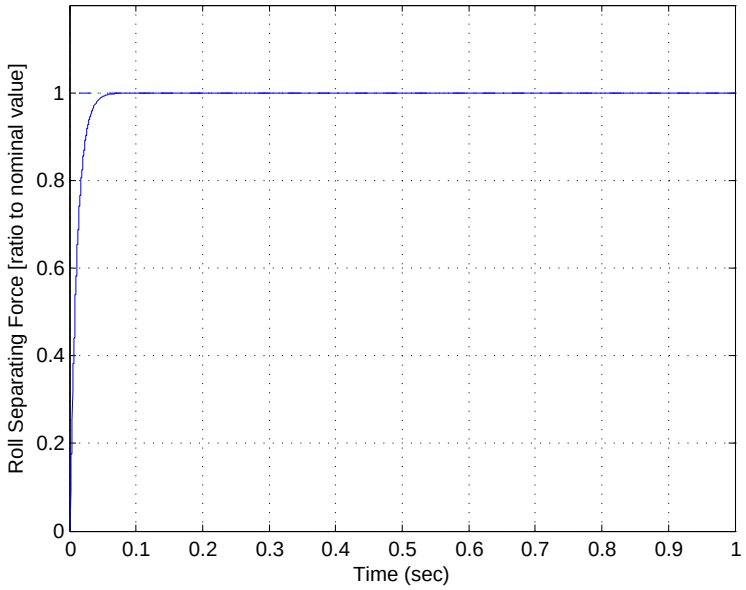

(a) Relative step response of roll separating force, $k_{p1} = 0.15$ and $k_{I1} = 7.5$

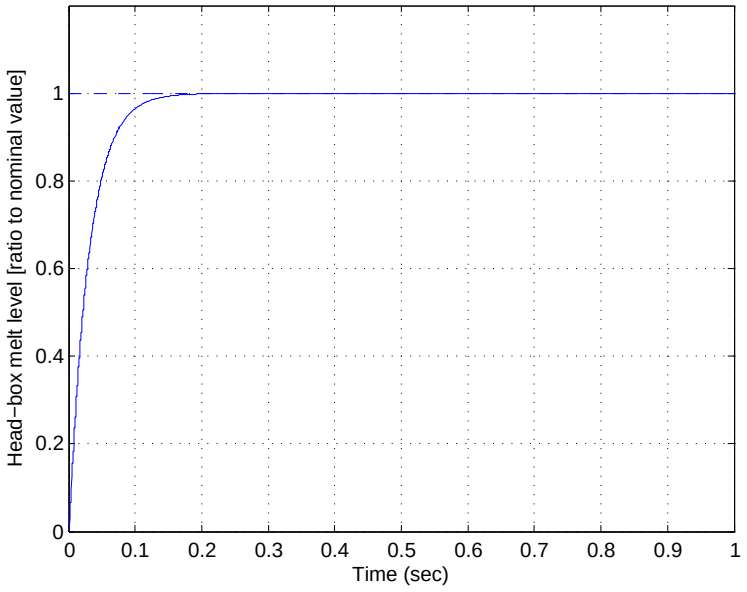

(b) Relative step response of head-box melt level, $k_{p2} = 2$ and $k_{I2} = 0.526$

Fig. 4.6 Relative reference step responses

The coupling between the head-box melt level and the roll separating force as expressed by the transfer function element $G_{12}(s)$ of the transfer matrix $\mathbf{G}(s)$ may lead to a deterioration in the time response and instability. To illustrate the effect of this coupling element on the controlled roll separating force, a step input equal to the operating point of the melt level is applied to the reference command r_2 only. The roll separating force time response as displayed in Fig. 4.7 exhibits a deterioration in the transient response because of the coupling element G_{12}.

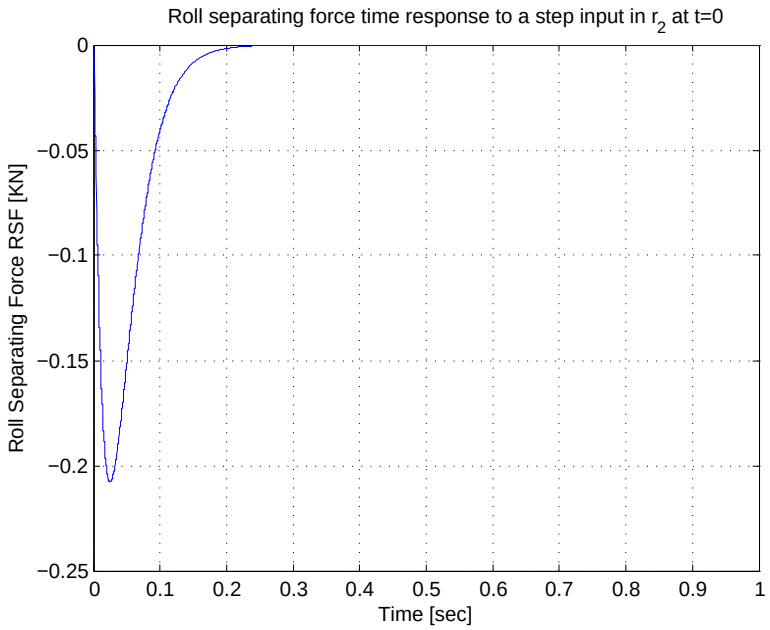

Fig. 4.7 The effect of the coupling element G_{12} on the RSF time response

Despite the aforementioned benefits and advantages of decentralized feedback control, decentralized control design is based on a two step procedure (an input-output pairing selection and a diagonal controller design) and more importantly the resulting controller is not unique. Moreover, decentralized control loops are often affected by set-point changes and interactions, which are treated as disturbances, from the other loops. Alternatively, the control problem can be formalized as an optimization problem to synthesize a multivariable

controller (centralized controller). In the next subsection, $\mathcal{H}_\infty$ design method is used to synthesize a multivariable controller $K(s)$.

4.3.2 $\mathcal{H}_\infty$ Optimal Control

4.3.2.1 Introduction

Before passing on to the $\mathcal{H}_\infty$ optimal control theory, it is worthwhile to briefly introduce some basic concepts and notions regarding $\mathcal{H}_\infty$, $\mathcal{H}_2$ norms. It is pertinent to note that all definitions and notions presented here are borrowed from [35],[37]. The spaces $\mathcal{H}_\infty$ and $\mathcal{H}_2$ designate the standard Hardy spaces which define the set of stable and (strictly) proper transfer functions and their norms are of great significance in control theory. One of the control design objectives is to render the sensitivity or its complementary function of a system small in the bandwidth of interest for disturbance attenuation and good tracking performance. For that purpose, $\mathcal{H}_\infty$-norm can be used to quantify the size of both signals and systems.

$\mathcal{H}_\infty$-norm of a system can be read as the maximum gain of the system and/or the maximum peak in the Bode diagram of a transfer function, see Fig. 4.8, whereas the squared $\mathcal{H}_2$-norm defines the energy in the impulse response of a system and can be read as the expected root-mean-square (RMS) value of the system's output.

$\mathcal{H}_\infty$-norm of a dynamic LTI system of an input u, an output y and a scalar transfer function G is given by

$$\|G\|_\infty \triangleq \max_{\omega\in\mathbb{R}} |\hat{g}(j\omega)|$$

where $|.|$ denotes the magnitude and $\hat{g}(j\omega)$ is the frequency response of G. There is no guarantee that the maximum exists or is attainable. The maximum, therefore, is replaced

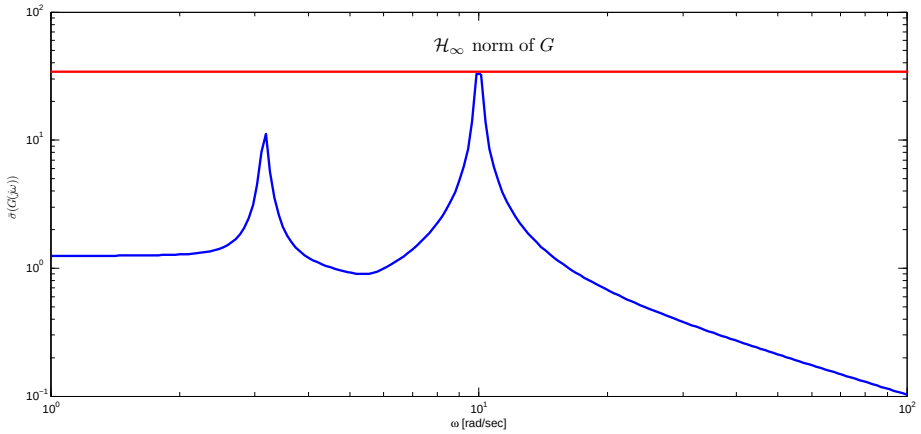

Fig. 4.8 $\mathcal{H}_\infty$-norm interpretation of a system $G(s)$

by a 'supremum'

$$\|G\|_\infty = \sup_{u \in \mathcal{L}_2} \frac{\|Gu\|_2}{\|u\|_2}$$

The above definition can be generalized to MIMO systems by considering singular value decomposition to quantify the size of a multivariable system and stability margins. Thus, the $\mathcal{H}_\infty$-norm of a transfer matrix $\mathbf{G}(s)$ is defined by

$$\|\mathbf{G}\|_\infty \triangleq \sup_{\omega \in \mathbb{R}} \bar{\sigma}(\mathbf{G}(j\omega))$$

where $\|.\|_\infty$ denotes $\mathcal{H}_\infty$-norm and $\bar{\sigma}(.)$ denotes the maximum singular value.

4.3.2.2 $\mathcal{H}_\infty$ Control Problem and Solution

$\mathcal{H}_\infty$ optimal control is a norm-based and model-based design technique. That is, the controller design depends on a plant model and the design technique is based on minimizing a norm. The $\mathcal{H}_\infty$ control problem is to synthesize a controller that minimizes the $\mathcal{H}_\infty$ norm of a closed loop transfer function and internally stabilizes the closed loop system. Two

different approaches for $\mathcal{H}_\infty$ controller design can be distinguished that are transfer function shaping approach (mixed-sensitivity $\mathcal{H}_\infty$ control) and signal- based approach [35]. However, the most significant result and elegant solution of the general $\mathcal{H}_\infty$ control problem is the seminal work of Doyle, Glover, Khargonekar and Francis [40]. The solution is referred to as the state-space solution and/or the 'DGKF- solution'. The general control configuration that forms the basis for synthesizing multivariable controllers using different methods such as $\mathcal{H}_\infty$, $\mathcal{H}_2$ and μ- optimal control is depicted in Fig. 4.9

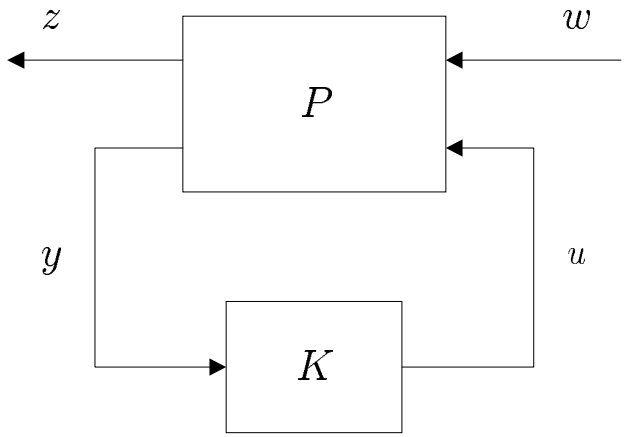

Fig. 4.9 General control configuration

where P designate the generalized plant (plant model G plus weighting functions), y is the measured outputs, u is the control inputs, w is the generalized disturbances (reference inputs, disturbance, noise) and z is the controlled outputs (error signals which need to be minimized). Therefore, the mathematical description of the closed loop system depicted in Fig. 4.9 is given by

$$\begin{bmatrix} z \\ y \end{bmatrix} = \begin{bmatrix} P_{11} & P_{12} \\ P_{21} & P_{22} \end{bmatrix} \begin{bmatrix} w \\ u \end{bmatrix}$$

$$u = K(s)y$$

Through linear fractional transformation, the closed loop transfer function $\mathcal{F}_\ell(P, K) : w \mapsto z$ reads as

$$\mathcal{F}_\ell(P, K) = P_{11} + P_{12}K(I - P_{22}K)^{-1}P_{21}$$

The $\mathcal{H}_\infty$ controller synthesis problem is to find a controller $K(s)$ such that $\mathcal{H}_\infty$ norm of $\mathcal{F}_\ell(P, K)$ is bounded by a constant value $\gamma > 0$ which represents the desired control performance of the closed loop system.

That is,

$$\|\mathcal{F}_\ell(P, K)\|_\infty := \sup_\omega \bar{\sigma}(\mathcal{F}_\ell(P, K)) < \gamma \tag{4.2}$$

or

$$\min_K \|\mathcal{F}_\ell(P, K)\|_\infty = \min_K \|M(K)\|_\infty$$

Let

$$P = \left[\begin{array}{c|cc} A & B_1 & B_2 \\ \hline C_1 & D_{11} & D_{12} \\ C_2 & D_{21} & D_{22} \end{array}\right]$$

be a state space realization of the generalized plant $P(s)$. The standard assumptions under which the $\mathcal{H}_\infty$ problem is synthesized and solved are:

- (A, B_1) is stabilizable (or even controllable) and (A, C_1) is detectable (or even observable).
- (A, B_2) is stabilizable and (A, C_2) is detectable .
- D_{21} has full row rank, and D_{12} has full column rank.
- $D_{11} = 0$ and $D_{22} = 0$.

- For all $\omega \in \mathbb{R}$, $\begin{pmatrix} A - j\omega I & B_1 \\ C_2 & D_{21} \end{pmatrix}$ has full row rank, and $\begin{pmatrix} A - j\omega I & B_2 \\ C_1 & D_{12} \end{pmatrix}$ has full column rank.
- $D_{12}^T \begin{pmatrix} C_1 & D_{12} \end{pmatrix} = \begin{pmatrix} 0 & I \end{pmatrix}$
- $D_{21} \begin{pmatrix} B_1^T & D_{21}^T \end{pmatrix} = \begin{pmatrix} 0 & I \end{pmatrix}$

Unlike the $\mathcal{H}_2$ control problem, where the $\mathcal{H}_2$ optimal controller is unique and can be found from solving two Algebraic Riccati Equations (ARE's), finding an $\mathcal{H}_\infty$ optimal controller is more complicated [35]. Thus, the minimization problem $\min_K \|M(K)\|_\infty$ can be solved numerically using the algorithm of Doyle et al. [40] by finding the smallest value of γ such that the Hamiltonian matrices have no eigenvalues on the imaginary axis. The algorithm was implemented in $MATLAB^{TM}$ using *hinfsyn* function.

Broadly speaking, there are several physical limitations and fundamental constraints imposed on a plant model such as RHP- poles and zeros, actuator saturation, model errors and more importantly 'S+T=I' which implies that it is not possible to simultaneously make the sensitivity and its complementary function small. Furthermore, if the sensitivity function is made small at low frequencies, the performance will deteriorate at high frequencies because the $\mathcal{H}_\infty$ norm compared to $\mathcal{H}_2$ norm presses the peak value (worst-case value) of the sensitivity function down but not the whole curve. Those limitations and constraints render the minimization problem of $\mathcal{H}_\infty$, as presented above in its pure form, not effective [41] because it treats all frequencies the same. Consequently, scaling using weighting functions, as depicted in Fig. 4.1, is used and they are incorporated in the $\mathcal{H}_\infty$ norm. The weighting functions, however, should be stable and minimum phase for the general $\mathcal{H}_\infty$ algorithm to be applicable. More importantly, they should not violate the fundamental constraint 'S+T=I' and should have stable inverses. In order to avoid violating the

fundamental equality, the perspective weights have to be appropriately chosen such that frequency responses of S and T intersect below zero-dB line [37].

The following discussion is based on [37] and [35]. In the signal- based $\mathcal{H}_\infty$ control approach, as the name implies, the design weights are chosen to characterize the frequency contents of the exogenous and error signals, whereas in the mixed sensitivity $\mathcal{H}_\infty$ control approach the weights are selected to shape the closed loop transfer functions such as S, T and/or KS in order to achieve the desired closed loop bandwidth and the required trade-offs. Recall that $S := \frac{1}{(1+GK)}$ is the sensitivity function mapping the reference command r to the error signal e, $T := \frac{GK}{(1+GK)} = 1 - S$, for SISO systems, is the complementary transfer function mapping r to the output y and KS is the control sensitivity mapping r to the control signal u. To illustrate how the $\mathcal{H}_\infty$ control design problem using mixed sensitivity approach is formulated, let us consider the example in Fig. 4.10 which shows the generalized plant P including different frequency-dependent weights and the actual plant G. The closed loop transfer function $M(K) = \mathcal{F}_\ell(P, K)$ from w to z which is to be minimized can be found as

$$\begin{bmatrix} z_1 \\ z_2 \\ z_3 \end{bmatrix} = \begin{bmatrix} W_1 S \\ W_2 T \\ W_3 K S \end{bmatrix} r = \mathcal{F}_\ell(P, K) r$$

Figure 4.10 can be cast into the general control structure as shown in Fig. 4.9. Thus, the generalized plant $P(s)$ can be written as

$$\left[\begin{array}{c} z_1 \\ z_2 \\ z_3 \\ \hline e \end{array}\right] = \left[\begin{array}{c|c} W_1 & -W_1 G \\ 0 & W_2 G \\ 0 & W_3 \\ \hline I & -G \end{array}\right] \left[\begin{array}{c} w \\ \hline u \end{array}\right] = \left[\begin{array}{c|c} P_{11} & P_{12} \\ \hline P_{21} & P_{22} \end{array}\right] \left[\begin{array}{c} w \\ \hline u \end{array}\right]$$

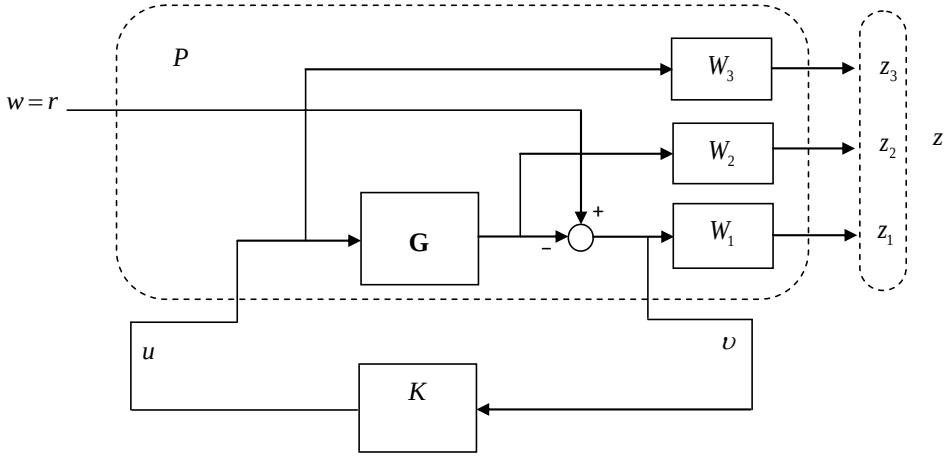

Fig. 4.10 Standard mixed-sensitivity minimization structure

Thus, the mixed sensitivity optimization problem is to find a stabilizing controller which minimizes

$$\|M(K)\|_\infty = \left\| \begin{bmatrix} W_1 S \\ W_2 T \\ W_3 K S \end{bmatrix} \right\|_\infty \tag{4.3}$$

Suppose that by tuning the weights W_1, W_2 and W_3, we have obtained $\|M(K)\|_\infty < \gamma$ Then:

$$\|W_1 S\|_\infty < \gamma \Rightarrow \forall\omega : |S(j\omega)| < \left|\gamma W_1^{-1}(j\omega)\right|$$

$$\|W_2 T\|_\infty < \gamma \Rightarrow \forall\omega : |T(j\omega)| < \left|\gamma W_2^{-1}(j\omega)\right|$$

$$\|W_3 K S\|_\infty < \gamma \Rightarrow \forall\omega : |KS(j\omega)| < \left|\gamma W_3^{-1}(j\omega)\right|$$

The weights are the tuning parameters which are iteratively adapted based on a good insight in the desired performance specifications. The appropriate choice of those weights is a typical engineering skill. However, they must all be stable otherwise the general $\mathcal{H}_\infty$

algorithm is not applicable. That being said, a good starting point is to choose

$$W_1(s) = \frac{s/M + \omega_0}{s + \omega_0 A};\ W_3(s) = const.$$

Where $A < 1$ is the maximum steady state offset; ω_0 is the desired bandwidth and M is the sensitivity peak. Similarly, a good starting point to choose W_2 is

$$W_2(s) = \frac{s + \omega_0/M}{As + \omega_0}$$

The inverses of W_1 and W_2 are the upper bounds on the desired sensitivity loop shape and the desired complementary sensitivity loop shape respectively. The inverse of W_3 is to limit the controller output u. In the next subsection, S/T mixed sensitivity optimization approach is applied to the CANMET-MTL TRC.

4.3.2.3 Application to the CANMET-MTL TRC

In this application, the mixed sensitivity design approach, one of the $\mathcal{H}_\infty$ optimal control design techniques, is adopted. The simple mixed sensitivity optimization setup depicted in Fig. 4.12 is viewed as a reference tracking problem, where $W_1(s) = diag\{w_{11}, w_{12}\}$ and $W_2(s) = diag\{w_{21}, w_{22}\}$ are diagonal matrices with stable transfer function weights to be chosen appropriately. The control problem is to design a stabilizing full multivariable controller

$$K(s) := \begin{bmatrix} K_{11}(s) & K_{12}(s) \\ K_{21}(s) & K_{22}(s) \end{bmatrix}$$

that minimizes reference tracking error and achieves good closed loop performance. Thus, the optimization problem is to find $K(s)$ to minimize the cost function

$$\left\| \begin{bmatrix} W_1 S \\ W_2 T \end{bmatrix} \right\|_\infty < \gamma \tag{4.4}$$

This cost function was considered by Imanari et al. [42] in the context of looper control of hot-strip mills. It is pertinent to note, however, that the weighting matrices are chosen to obtain a good closed loop performance rather than represent model errors or unmodelled dynamics. In other words, the $\mathcal{H}_\infty$ optimal controller is designed to maintain the nominal performance (i.e. setting the uncertainty block Δ in Fig. 4.11 null).

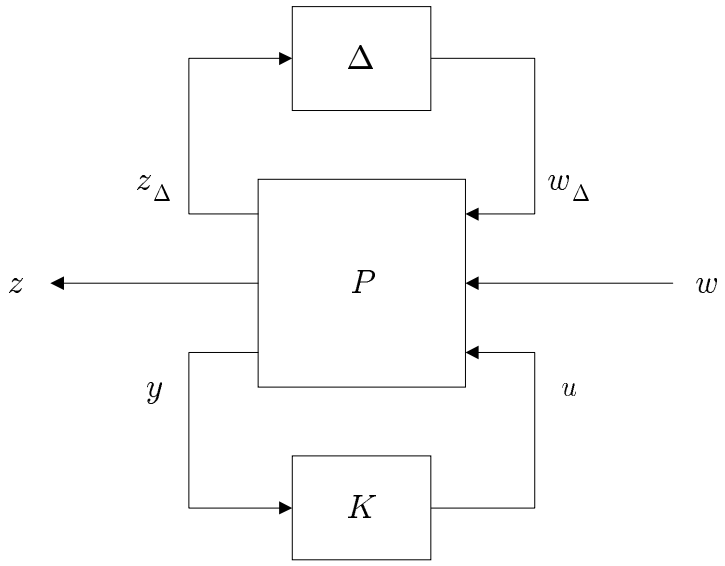

Fig. 4.11 General closed loop interconnection with uncertainty block

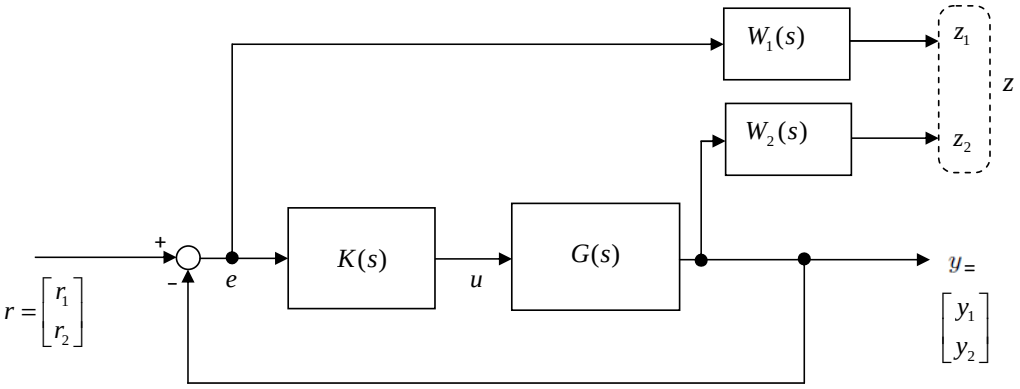

Fig. 4.12 S/T mixed-sensitivity optimization structure

For tracking problem, the classic control design using PI-controllers demonstrated a zero-steady state in each of the controlled outputs. It would be desirable to include integral terms $\frac{1}{s}$ in the weights associated with the tracking error of each loop in order to minimize the sensitivity S at low frequencies and reflect those integral actions in the controller. However, the standard $\mathcal{H}_\infty$ optimal control problem would not be well-posed if pure integrators are included in W_1 [35]. Therefore, we could penalize the tracking error via $W_1 S$ by choosing the weighting functions to be low-pass filters with a crossover frequency approximately equal to that of the desired closed loop bandwidth of each loop. Different bandwidth can be achieved for each loop. In this application, however, same bandwidth of 20 rad/s is desired for each closed loop. Selecting the steady state offset A in W_1 to be smaller than 1 enforces approximate integral actions in each of the controlled outputs. Thus, the selected W_1 reads as

$$W_1 = diag\left\{ \; 0.5\tfrac{s+40}{s+0.025}, \quad 0.5\tfrac{s+40}{s+0.025} \; \right\}$$

Shaping the complementary transfer function is desirable for tracking problems, noise attenuation and robust stability against output multiplicative uncertainty. In this application,

the objective of the weighting matrix W_2 is to make T small at high frequencies by adding additional roll-off in $L := (I + GK)$ to achieve better tracking. Thus, the magnitude of each transfer function elements of W_2 is selected to be small at low frequencies and large at high frequencies. High-pass filters with a crossover frequency approximately equal to that of the desired closed loop bandwidth 20 rad/s of each loop are chosen to form the matrix W_2

$$W_2 = diag\left\{ \begin{array}{cc} \frac{s+\frac{20}{2}}{\frac{1}{800}s+20}, & \frac{s+\frac{20}{2}}{\frac{1}{800}s+20} \end{array} \right\}$$

The $\mathcal{H}_\infty$ optimal controller design is carried out using MATLAB *hinfsyn* function. Thus, the standard $\mathcal{H}_\infty$ optimization problem defined by (4.4) is solved and a suboptimal controller achieving $\gamma = 1.12$ is obtained.

For the controller designed using the above weights, the frequency responses can be evaluated by plotting singular values of S and T over various frequencies. Singular value plots of sensitivity S and complementary sensitivity T functions along with their bounds are displayed in Fig. 4.13. It can be seen that the selected weights achieves the fundamental inequality 'S+T=I' as the singular value plots of W_1 and W_2 intersect at 0-dB line. Also, the desired closed bandwidth is achieved.

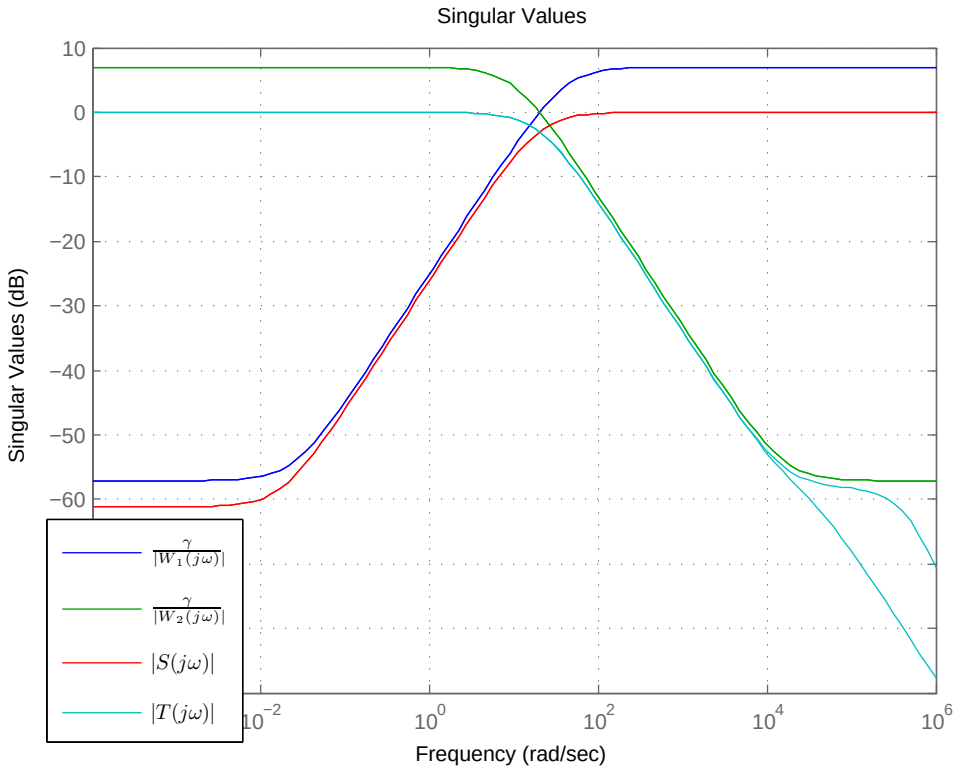

Fig. 4.13 Singular values of S and T and their bounds ($\gamma = 1.12$)

Step inputs equal to the operating points of roll separating force and melt level are simultaneously applied to the reference commands of $r_1 = f_{ref}$ and $r_2 = h_{ref}$. Simulation results are presented in Fig. 4.14. Step responses show no steady state error in each of the controlled outputs. Moreover, step responses are considerably fast because the step response of roll separating force as shown in Fig. 4.14(a) reaches its final value in 0.4 s, whereas the reference step response of the head-box melt level as shown in Fig. 4.14(b) reaches its final value in 0.3 s. The controller outputs u_1 and u_2 are shown in Fig. 4.15. The resulting $\mathcal{H}_\infty$ optimal controller is a 2×2 transfer matrix of sixth order minimal transfer function elements. Typically, $\mathcal{H}_\infty$ synthesis technique results in a high dimensional controller. For the sake of brevity, only K_{11} is given here

$$K_{11} = \frac{3.288\times10^{7}s^{5}+3.834\times10^{13}s^{4}+1.085\times10^{19}s^{3}+1.639\times10^{23}s^{2}+1.216\times10^{24}s+2.12\times10^{22}}{s^{6}+1.194\times10^{8}s^{5}+1.401\times10^{14}s^{4}+4.128\times10^{19}s^{3}+1.21\times10^{24}s^{2}+4.229\times10^{22}s+3.694\times10^{20}}$$

The absence of RHP-zeros from the plant model explains the high gains of the resulting optimal controller. It is evident from the step responses that the resulting controller achieves good reference tracking behaviour and good closed loop performance.

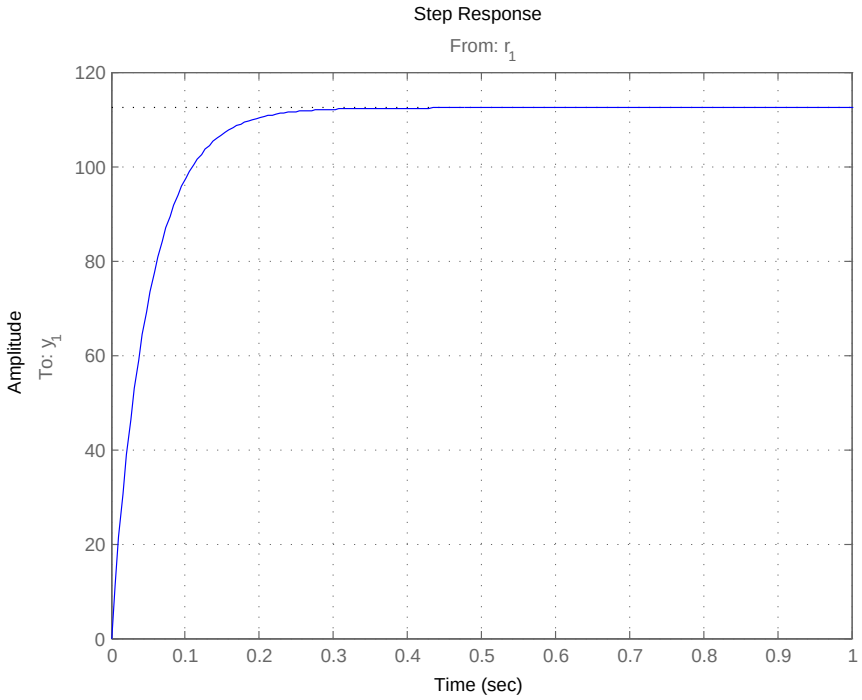

(a)

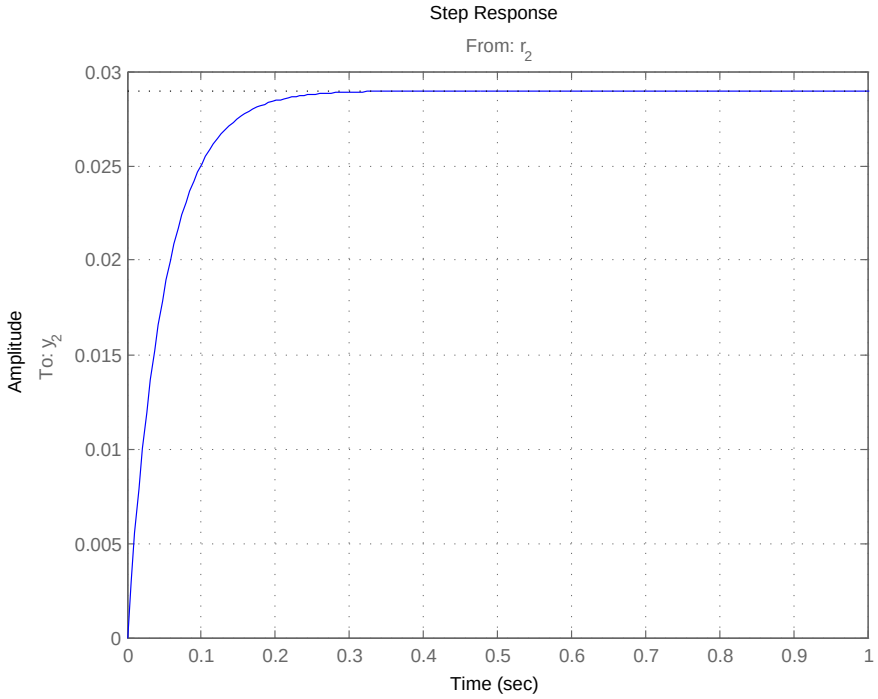

(b)

Fig. 4.14 Step responses of (a) roll separating force and (b) head-box melt level ($\gamma = 1.12$)

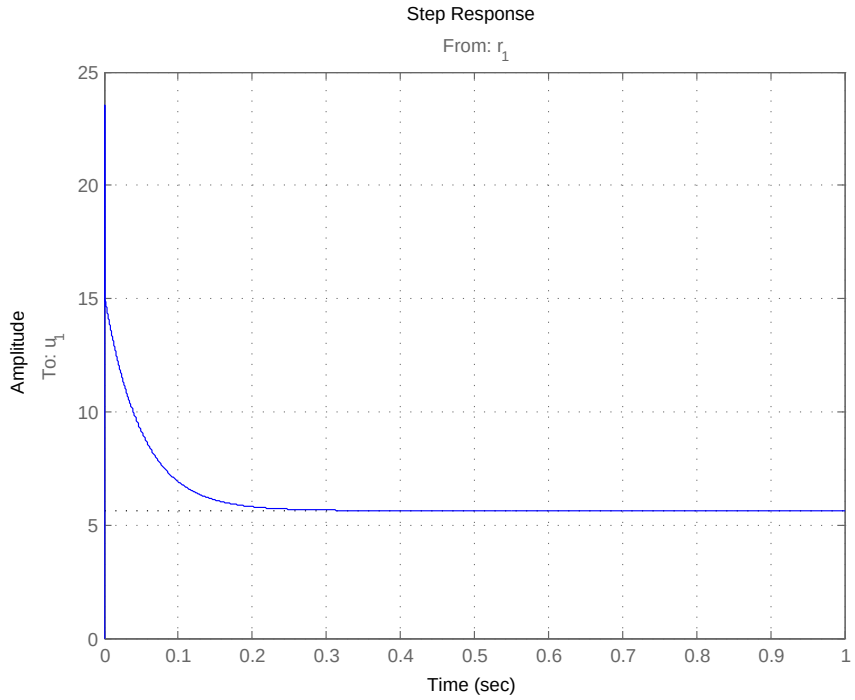

(a)

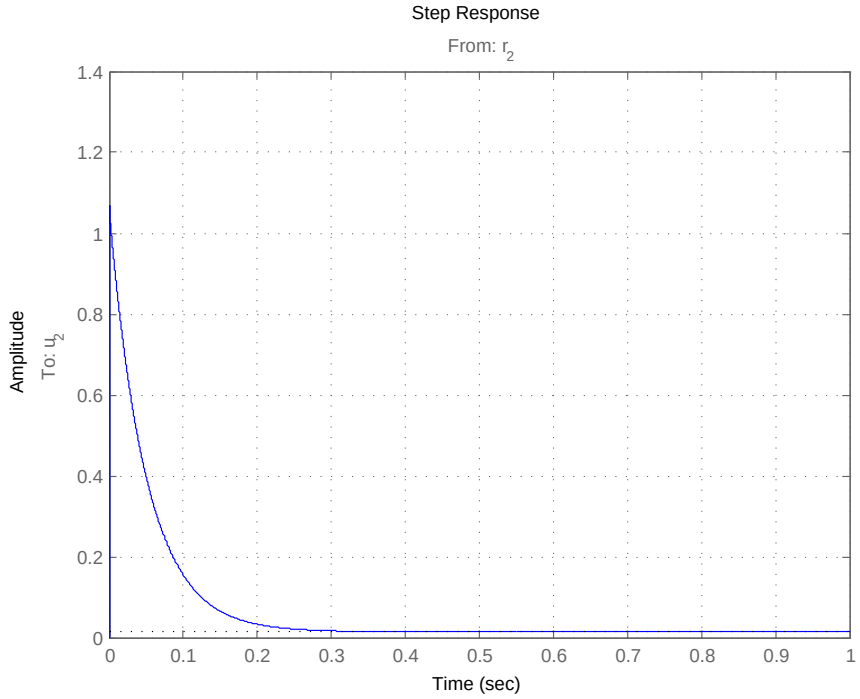

(b)

Fig. 4.15 Step responses from (a) $r_1 \longmapsto u_1$ and (b) $r_2 \longmapsto u_2$ ($\gamma = 1.12$)

The cost function given in (4.4) can be further minimized by adjusting the design weights such that $\mathcal{H}_\infty$ *gamma* becomes smaller than one, but this comes at the price of sluggish step responses. The control design is carried out again with different design weights and a controller achieving $\gamma = 0.5$ is obtained. The adjusted weights are given as follows

$$W_1 = \frac{0.1s + 1}{s + 0.001} I_2,$$

I_2 is identity matrix

$$W_2 = diag \left\{ \begin{array}{cc} \frac{s+\frac{20}{2}}{\frac{1}{800}s+20}, & \frac{s+\frac{40}{2}}{\frac{1}{800}s+40} \end{array} \right\}$$

For the controller achieving $\gamma = 0.5$, singular value plots of sensitivity S and complementary sensitivity T functions along with their bounds are displayed in Fig. 4.16 and the closed loop step responses of roll separating force and melt level are displayed in Fig. 4.17. As it can be seen, the reference step responses in Fig. 4.17 are much sluggish than those are displayed in Fig. 4.14. The control signal plots of the resulting controller are displayed in Fig. 4.18

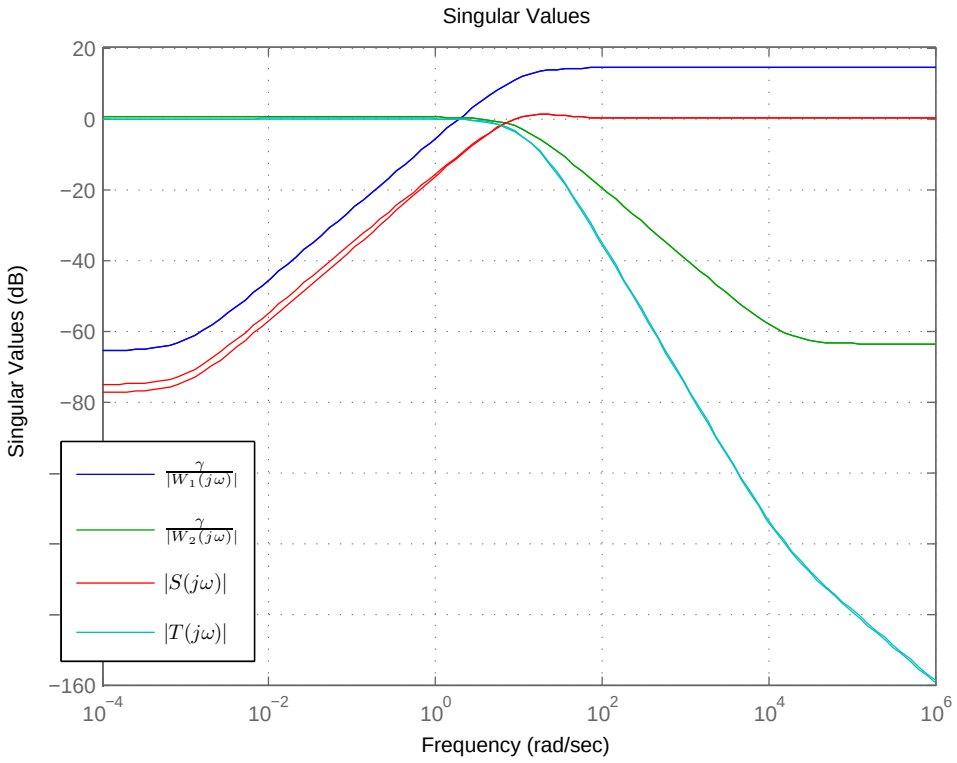

Fig. 4.16 Singular values of S and T and their bounds ($\gamma = 0.5$)

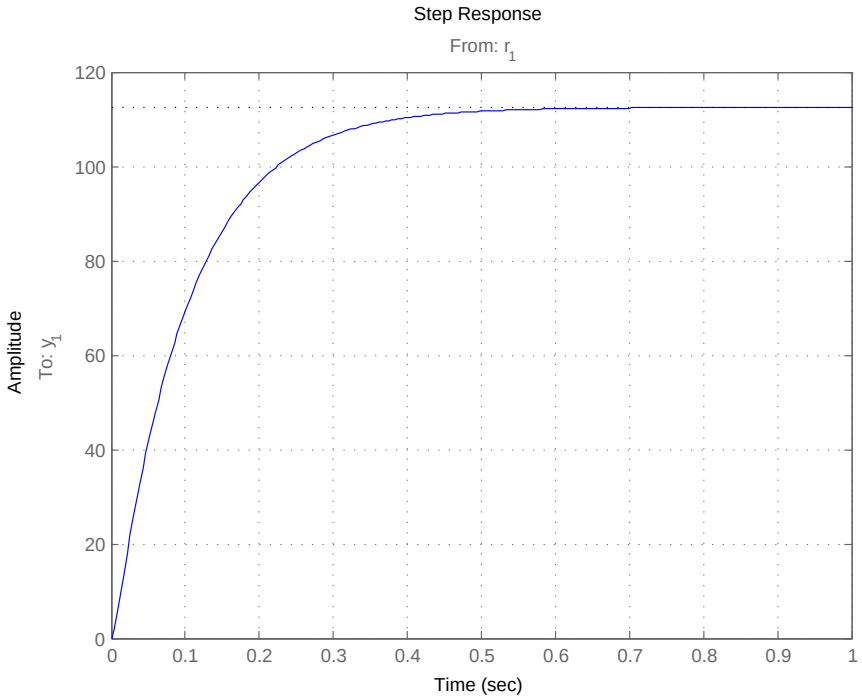

(a)

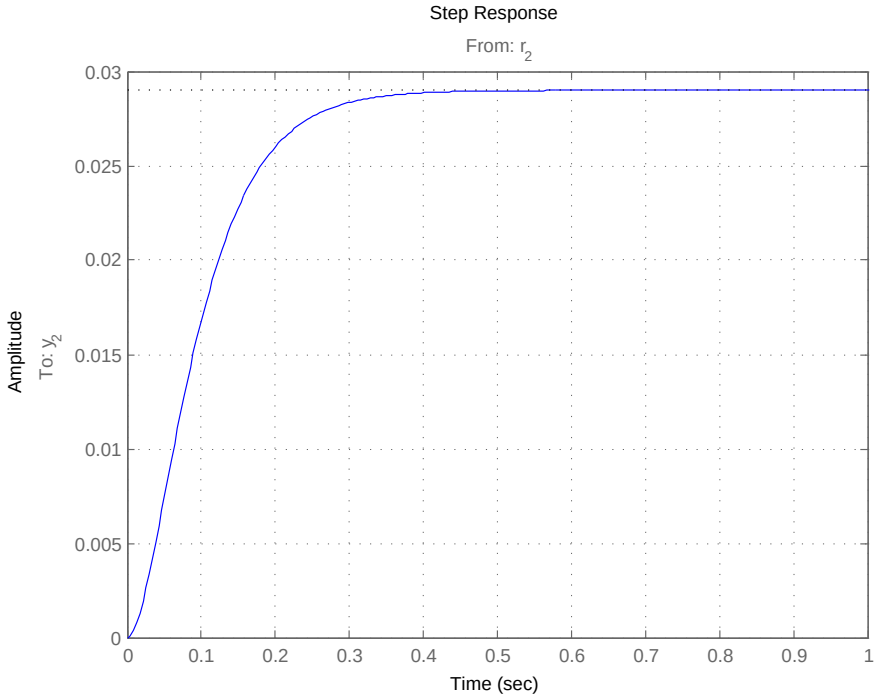

(b)

Fig. 4.17 Step responses of (a) roll separating force and (b) head-box melt level ($\gamma = 0.5$)

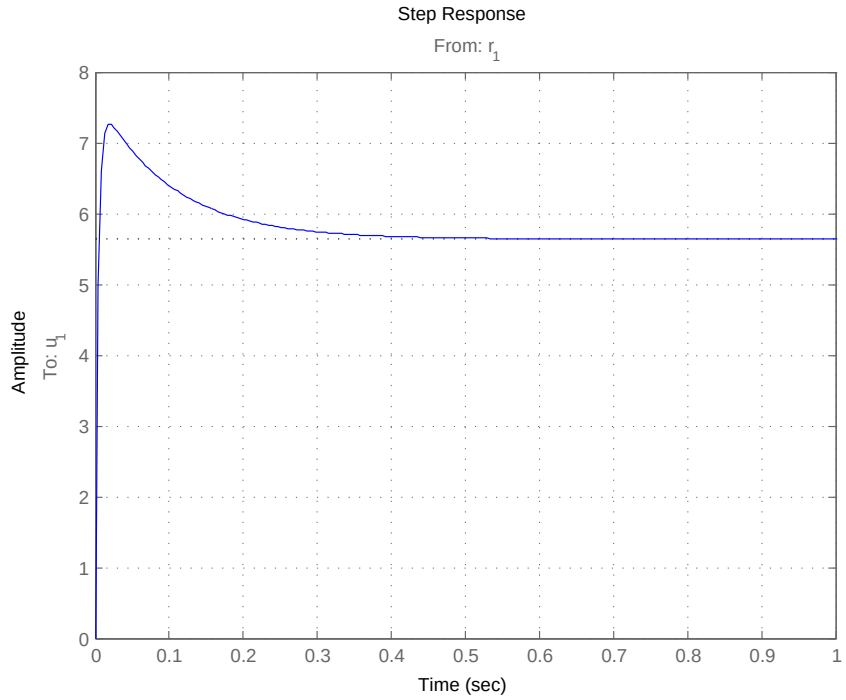

(a)

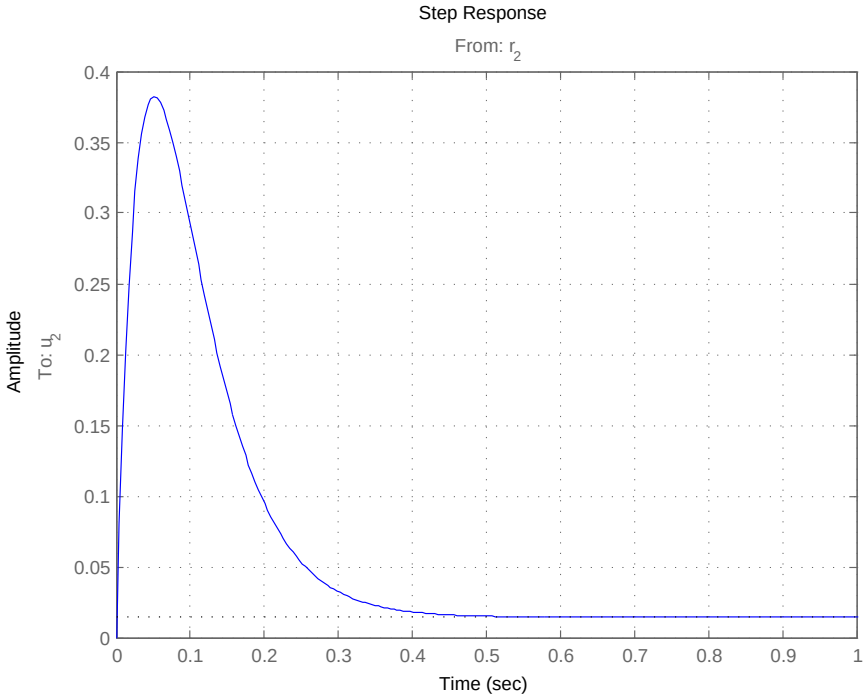

(b)

Fig. 4.18 Step responses from (a) $r_1 \longmapsto u_1$ and (b) $r_2 \longmapsto u_2$ ($\gamma = 0.5$)

4.4 Summary

In this chapter, the dynamical characteristics of the proposed model derived in Chapter 3 was analysed. It has been found that plant model is diagonally dominant. Therefore, there is no need for decoupling pre-compensator design. A decentralised diagonal controller (SISO controllers) was designed and independently tuned for each control loop. The PI-decentralised controllers demonstrated good reference tracking capability even though the plant model with diagonal dominance is partly coupled. $\mathcal{H}_\infty$ control theory was briefly reviewed. Despite the result that the coupling between the inputs and the outputs of the plant model is weak and modest, a full multivariable controller was designed and simulation results have been displayed. The simulation results showed that good reference tracking is feasible using multivariable control. Nonetheless, $\mathcal{H}_\infty$ synthesis led to high-dimensional controllers which render the hardware implementation of the controllers difficult and their retuning is not easy for operators. Thus, model reduction is needed to scale down the controllers to lower order. On the contrary, the two-step technique (decentralized feedback control) is easy to implement, maintain and is commonly used in practice.

Chapter 5

Conclusion

A summary of the main salient results and a collection of several possible directions for future research conclude this thesis.

5.1 Summary

A horizontal magnesium twin-roll strip casting machine housed at the CANMET Materials Technology Laboratories (CANMET-MTL), Hamilton- Canada has been considered for modelling and control. The dynamics of the proposed plant model has been analysed. Decentralised (SISO) controllers and fully centralised (multivariable) controller have been designed. The CANMET-MTL TRC machine is modelled as a 2×2 linear parameter-varying transfer matrix. Despite the fact that the model has not been validated due to the lack of experimental data from the TRC machine, the mathematical model derived gives a good insight into the fundamental dynamics and features of the TRC machine. Furthermore, it is attractive for control synthesis with frequency domain design methods. It has been found that the dynamics of the proposed model changes with the casting speed

operating range. An admissible casting speed range has been obtained for different casting configurations by solving non-linear model equation verified using numerical simulation data which is provided by a research group at the University of Waterloo. The obtained results in table 3.1 and 3.2 showed that the numerical model represented by the simulation data and the derived model equations are in good agreement. Also, as the roll gap, which is assumed to be constant and to define the final strip thickness, decreases the casting speed range increases. Regards optimizing the caster design, this may mean that casting at a thinner-gauge thickness can be more profitable than casting at a relatively large thin-gauge because of the increase in the production rate (i.e. casting speed). Moreover, the acceptable range of the casting speed increases as the setback distance increases. A casting configuration that provides 50% reduction in thickness was considered; a roll gap of 6 mm and a setback of 32.5 mm were chosen. From the carried analysis point of view, the proposed plant model for a 'nominal' casting speed of 2 m/min is stable and minimum phase with high static gains. A zero-frequency scaling was performed on the actual plant model of deviation variables to render the analysis much simpler. The RGA- based analysis suggested that a decentralised control design is possible with diagonal pairings. Therefore, A PI-decentralised controller was designed and independently tuned for melt level control loop and roll-separating force loop. The PI-decentralized controllers displayed good reference tracking capability due to the result that the proposed transfer matrix is non-singular at zero frequency and the coupling between the inputs and outputs is partial and modest. Thus, the 2×2 system was considered as two SISO subsystems. The $\mathcal{H}_\infty$ mixed sensitivity approach was adopted to design a full multivariable controller to maintain the nominal performance. The centralized multivariable controller led to good closed loop responses and zero steady state response was achieved for each of the controlled outputs. After all, both control structures (centralised and decentralised) provided good reference tracking.

However, as the casting operating condition changes, there is a need for fast, simple design technique that can be frequently repeated to maintain the nominal performance. In that sense, the decentralised control structure is preferable. Moreover, decentralised control structure is easy to implement, maintain and very effective in practice.

5.2 Future Directions

In regards of mathematical modelling, controlling the roll separating force and melt level in the head-box is of great importance in determining final strip thickness and quality of strip surfaces. The roll separating force is given as a function of solidification front position (kiss point of solidification front position) which in turn is influenced by a number of processing parameters such as molten level, casting speed, casting temperature, cooling water temperature and roll gap [33]. Nevertheless, measuring solidification front position is impractical. Therefore, finding an explicit expression for the solidification front position in terms of the foregoing processing parameters would improve the accuracy of the formulated model herein. This explicit mathematical expression could be found through carrying out extensive numerical simulations using highly effective numerical tools such as COMSOL multiphysics. Furthermore, if we want to lead the research into different direction that would ensure model accuracy, one could make use of numerical models (referred to as virtual process models), which are typically not adequate for control synthesis because they are of high order, to build more suitable mathematical models for feedback control using model reduction techniques. Nevertheless, these numerical models have to be experimentally validated using experimental data. However, large-scale experimental data is not yet made available for magnesium twin roll caster and the research at CANMET-MTL laboratory is still in its infancy when it comes to defining the optimal operating conditions. For

further details on utilizing virtual process models in control design, the interested reader is referred to [43] in which a 3-D finite element model (virtual process model) has been formulated for a low-pressure die casting process used for aluminium alloy wheels industry and a model predictive controller has been developed to regulate die temperatures. As for control design, the dynamics of the proposed plant model changes with the operating casting speed. Therefore, it might be of interest to design several controllers for different casting speeds using a gain-schedule approach or self-tuning technique. Another possibility is to use a robust control approach to design a multivariable controller that takes the dynamic variations into account. The uncertainty bounds can be obtained from the admissible range of the operating casting speed. The idea is to design a single controller that achieves acceptable performance for every admissible process transfer matrix.

References

[1] H. Müller, *Continuous casting: proceedings of the International Conference on Continuous Casting of Non-Ferrous Metals*. Wiley-VCH, 2006.

[2] T. Matsushita, "Development and commercialization of twin roll strip caster," *Facilities*, vol. 5, p. 6, 2009.

[3] "Canmet materials technology laboratory settling into new hamilton facility." `http://www.nrcan.gc.ca/minerals-metals/highlights/3236`, Jul. 2011. [Mar. 25, 2012].

[4] H. Bessemer, July 25, 1865.

[5] Y. Park and H. Cho, "A fuzzy logic controller for the molten steel level control of strip casting processes," *Control Engineering Practice*, vol. 13, no. 7, pp. 821 – 834, 2005. Control Applications of Optimisation.

[6] J. L. Hunter, "Method and apparatus for the continuous casting of metal." Hunter Enginnering Co., April 30, 1957.

[7] B. Li, "Producing thin strips by twin-roll casting part *i*: Process aspects and quality issues," *JOM Journal of the Minerals, Metals and Materials Society*, vol. 47, pp. 29–33, 1995. 10.1007/BF03221172.

[8] M. Ferry, M. Institute of Materials, and Mining, *Direct strip casting of metals and alloys: processing, microstructure and properties*. Woodhead publishing in materials, Woodhead Pub. and Maney Pub. on behalf of The Institute of Materials, Minerals & Mining, 2006.

[9] E. Romano and C. Romanowski, "Reinventing twin roll casting for the 21^{st} century," in *Cast Shop for Aluminum Production* (G. Bearne, ed.), p. 895, TMS (The Minerals, Metals & Materials Society), 2009.

[10] D. Liang and C. Cowley, "The twin-roll strip casting of magnesium," *JOM Journal of the Minerals, Metals and Materials Society*, vol. 56, pp. 26–28, 2004. 10.1007/s11837-004-0122-6.

[11] H. Watari, T. Haga, N. Koga, and K. Davey, "Feasibility study of twin roll casting process for magnesium alloys," *Journal of Materials Processing Technology*, vol. 192-193, pp. 300–305, 2007.

[12] J. Zeng, R. Koitzsch, H. Pfeifer, and B. Friedrich, "Numerical simulation of the twin-roll casting process of magnesium alloy strip," *Journal of Materials Processing Technology*, vol. 209, no. 5, pp. 2321 – 2328, 2009.

[13] H. Fredriksson and U. Åkerlind, *Materials processing during casting*. Wiley, 2006.

[14] C. A. Romanowski, A. Duw Uri, W. E. Carey, and W. M. Marrison, "Thin gauge roll casting method and apparatus," 2000.

[15] D. S. LEE, J. S. LEE, and T. KANG, "Robust molten steel level control in a strip-casting process," *ISIJ International*, vol. 45, no. 8, pp. 1165–1172, 2005.

[16] D. Lee, J. Lee, and T. Kang, "Adaptive fuzzy control of the molten steel level in a strip-casting process," *Control Engineering Practice*, vol. 4, no. 11, pp. 1511 – 1520, 1996.

[17] D. M. Lee, *adaptive fuzzy control to systems with state dependent input gain*. PhD thesis, Pohang University of Science and Technology, 1997.

[18] S. Bernhard, M. Enning, and H. Rake, "Automation of a laboratory plant for direct casting of thin steel strips," *Control Engineering Practice*, vol. 2, no. 6, pp. 961 – 967, 1994.

[19] F. Simon, S. Bernhard, and H. Rake, "Gain scheduled pi-control of strip casting plant," *IFAC Conference on Control of Industrial Systems*, vol. 3, pp. 1179–1184, 1997.

[20] K.-S. Hong, S.-H. Kim, and K.-I. Lee, "An integrated control of strip casting process by decentralization and optimal supervision," in *American Control Conference, 1998. Proceedings of the 1998*, vol. 2, pp. 723 –727 vol.2, jun 1998.

[21] K.-S. Hong, J.-G. Kim, and M. Tomizuka, "Control of strip casting process: decentralization and optimal roll force control," *Control Engineering Practice*, vol. 9, no. 9, pp. 933 – 945, 2001. Review Papers on Automation in Mineral and Metal Processing.

[22] J. B. Edwards, "Interaction analysis of the twin-roller strip-casting process and the implications for process control," *Journal of materials engineering and performance*, vol. 14, no. 3, p. 395, 2005.

[23] A. Cavazos, "Multivariable $\mathcal{H}_\infty$ force/level control of the twin-roller strip caster," *Arabian journal for science and engineering. Section B: Engineering*, vol. 30, no. 1, p. 57, 2005.

[24] C. Alberto, "Considerations for multivariable control of the twin-roller strip caster," *ISA Transactions*, vol. 45, no. 2, pp. 271 – 294, 2006.

[25] "Materials technology." `http://www.nrcan.gc.ca/minerals-metals/materials-technology/2945`, Jul. 2011. [Mar. 29, 2012].

[26] B. Li, "Producing thin strips by twin-roll casting part ii: Process modeling and development," *JOM Journal of the Minerals, Metals and Materials Society*, vol. 47, pp. 13–17, 1995. 10.1007/BF03221451.

[27] C. A. Santos, J. A. Spim Jr, and A. Garcia, "Modeling of solidification in twin-roll strip casting," *Journal of Materials Processing Technology*, vol. 102, no. 1-3, pp. 33–39, 2000.

[28] H. Zhao, P. Li, and L. He, "Coupled analysis of temperature and flow during twin-roll casting of magnesium alloy strip," *Journal of Materials Processing Technology*, vol. 211, no. 6, pp. 1197 – 1202, 2011.

[29] A. S. M. I. H. Committee, "Asm handbook, volume 15 - casting." ASM International.

[30] M. Hanao, M. Kawamoto, and A. Yamanaka, "Growth of solidified shell just below the meniscus in continuous casting mold," *ISIJ International*, vol. 49, no. 3, pp. 365–374, 2009.

[31] Y. Kim, D. Lee, M. Joo, T. Kang, and K. Paek, "Control problem and solution in the steady state in the strip casting process," in *Industrial Electronics, 2001. Proceedings. ISIE 2001. IEEE International Symposium on*, vol. 1, pp. 520 –525 vol.1, 2001.

[32] W. P. Weng, K. Deng, Z. M. Ren, Q. Chen, Z. D. Chi, and Q. T. Zhao, "Kiss-point position control of solidification layer and process optimization for twin-roll casting of magnesium alloys," *Advanced Materials Research*, vol. 189-193, pp. 3844–3851, 2011.

[33] G.-m. Cao, C.-g. Li, G.-p. Zhou, Z.-y. Liu, D. Wu, G.-d. Wang, and X.-h. Liu, "Rolling force prediction for strip casting using theoretical model and artificial intelligence," *Journal of Central South University of Technology*, vol. 17, pp. 795–800, 2010. 10.1007/s11771-010-0558-5.

[34] O. Vivero and J. Liceaga-Castro, "Mimo toolbox for matlab," in *Student Paper, 2008 Annual IEEE Conference*, pp. 1 –5, feb. 2008.

[35] S. Skogestad and I. Postlethwaite, *Multivariable feedback control: analysis and design*. John Wiley, 2005.

[36] K. Johansson and A. Rantzer, "Decentralized control of sequentially minimum phase systems," *Automatic Control, IEEE Transactions on*, vol. 44, pp. 1909 –1913, oct 1999.

[37] A. Damen and S. Weiland, "Robust control." Eindhoven University of Technology, Lecture notes, July 2002.

[38] P. Campo and M. Morari, "Achievable closed-loop properties of systems under decentralized control: conditions involving the steady-state gain," *Automatic Control, IEEE Transactions on*, vol. 39, pp. 932 –943, may 1994.

[39] G. Zames and D. Bensoussan, "Multivariable feedback, sensitivity, and decentralized control," *IEEE Transactions on Automatic Control*, vol. 28, no. 11, pp. 1030–1035, 1983.

[40] J. Doyle, K. Glover, P. Khargonekar, and B. Francis, "State-space solutions to standard h_2 and h_∞ control problems.," *Automatic Control, IEEE Transactions on*, vol. 34, pp. 831 –847, aug 1989.

[41] H. Kwakernaak, "Robust control and $\mathcal{H}_\infty$optimization−tutorial paper," *Automatica*, vol. 29, no. 2, pp. 255 – 273, 1993.

[42] H. Imanari, Y. Morimatsu, K. Sekiguchi, H. Ezure, R. Matuoka, A. Tokuda, and H. Otobe, "Looper h-infinity control for hot-strip mills," *Industry Applications, IEEE Transactions on*, vol. 33, pp. 790 –796, may/jun 1997.

[43] D. Maijer, W. Owen, and R. Vetter, "An investigation of predictive control for aluminum wheel casting via a virtual process model," *Journal of Materials Processing Technology*, vol. 209, no. 4, pp. 1965 – 1979, 2009.